



Contents lists available at ScienceDirect

European Journal of Medicinal Chemistry

journal homepage: <http://www.elsevier.com/locate/ejmech>

Research paper

Targeting nuclear protein TDP-43 by cell division cycle kinase 7 inhibitors: A new therapeutic approach for amyotrophic lateral sclerosis

Elisa Rojas-Prats ^{a,1}, Loreto Martinez-Gonzalez ^{a,1}, Claudia Gonzalo-Consuegra ^b, Nicole F. Liachko ^{c,d}, Concepción Perez ^e, David Ramírez ^f, Brian C. Kraemer ^{c,d,g,h}, Ángeles Martin-Requero ^{a,i}, Daniel I. Perez ^a, Carmen Gil ^{a,i}, Eva de Lago ^{b,i,**}, Ana Martinez ^{a,i,*}

^a Centro de Investigaciones Biológicas Margarita Salas-CSIC, Ramiro de Maeztu 9, 28040, Madrid, Spain

^b Instituto Universitario de Investigación en Neuroquímica, Departamento de Bioquímica y Biología Molecular, Facultad de Medicina, Universidad Complutense, Madrid, Spain

^c Department of Medicine, Division of Gerontology and Geriatric Medicine, University of Washington, Seattle, WA, 98104, USA

^d Geriatrics Research Education and Clinical Center, Veterans Affairs Puget Sound Health Care System, Seattle, WA, 98108, USA

^e Instituto de Química Médica-CSIC, Juan de La Cierva 3, 28006, Madrid, Spain

^f Instituto de Ciencias Biomédicas, Universidad Autónoma de Chile, Llano Subercaseaux 2801 – Piso 6, Santiago, Chile

^g Department of Psychiatry and Behavioral Sciences, University of Washington, Seattle, WA, 98195, USA

^h Department of Pathology, University of Washington, Seattle, WA, 98195, USA

ⁱ Centro de Investigación Biomédica en Red de Enfermedades Neurodegenerativas (CIBERNED), Instituto de Salud Carlos III, 28031, Madrid, Spain

ARTICLE INFO

Article history:

Received 16 July 2020

Received in revised form

15 October 2020

Accepted 23 October 2020

Keywords:

CDC7 inhibitors

TDP-43

ALS

FTLD

Drug discovery

ABSTRACT

Amyotrophic lateral sclerosis (ALS) is a fatal neurodegenerative disease with no known cure. Aggregates of the nuclear protein TDP-43 have been recognized as a hallmark of proteinopathy in both familial and sporadic cases of ALS. Post-translational modifications of this protein, include hyperphosphorylation, cause disruption of TDP-43 homeostasis and as a consequence, promotion of its neurotoxicity. Among the kinases involved in these changes, cell division cycle kinase 7 (CDC7) plays an important role by directly phosphorylating TDP-43. In the present manuscript the discovery, synthesis, and optimization of a new family of selective and ATP-competitive CDC7 inhibitors based on 6-mercaptapurine scaffold are described. Moreover, we demonstrate the ability of these inhibitors to reduce TDP-43 phosphorylation in both cell cultures and transgenic animal models such as *C. elegans* and Prp-hTDP43 (A315T) mice. Altogether, the compounds described here may be useful as versatile tools to explore the role of CDC7 in TDP-43 phosphorylation and also as new drug candidates for the future development of ALS therapies.

© 2020 Elsevier Masson SAS. All rights reserved.

Abbreviations: ALS, amyotrophic lateral sclerosis; BBB, Blood brain barrier; ATP, adenosine triphosphate; CDC7, Cell division cycle kinase 7; Dbf4, Dumbbell former 4 protein; EA, ethacrynic acid; FTLD, frontotemporal lobar degeneration; PAMPA, parallel artificial membrane permeability assay; PDB, protein data bank; SOD-1, superoxide dismutase 1; TDP-43, transactive response DNA binding protein of 43 kDa; TR-FRET, Time-resolved fluorescence energy transfer.

* Corresponding author. CIB-CSIC, Ramiro de Maeztu 9, 28040, Madrid, Spain.

** Corresponding author. Dpto. Bioquímica y Biología Molecular, Facultad de Medicina, UCM, Plaza Ramon y Cajal s/n, Ciudad Universitaria, 28040, Madrid, Spain.

E-mail addresses: elagofem@ucm.es (E. de Lago), ana.martinez@csic.es (A. Martinez).

¹ Equal contribution.

<https://doi.org/10.1016/j.ejmech.2020.112968>

0223-5234/© 2020 Elsevier Masson SAS. All rights reserved.

1. Introduction

Amyotrophic lateral sclerosis (ALS) is a fatal and devastating neurodegenerative disease that features the progressive loss of cortical and spinal motor neurons, leading to muscle weakness and spasticity as main clinical symptoms [1]. Classified as an orphan disease, ALS affects more than 800,000 patients worldwide with an estimated incidence of 1.5–2.7 per 100,000 people in Europe and North America. Despite important advances in the understanding of ALS molecular pathobiology, the etiology remains unknown. Today, ALS is considered a complex disease where a multifactorial combination of environmental and genetic factors may be involved

in its origin [2]. There is no cure for ALS and only riluzole and more recently edaravone are approved for their palliative treatment with limited results for the patients; thus, there is an urgent need to find an effective treatment [3].

Pathologically, several distinct aggregating proteinopathies have been described in patients with ALS. Aggregates of superoxide dismutase 1 (SOD1) were first identified in patients with mutations in this detoxifying enzyme [4]. In fact, the discovery that the SOD1 G93A mutation causes ALS in the beginning of the 90's allowed the development of the first transgenic mouse used in drug discovery for ALS [5]. However, only between the 5–10% of the ALS cases are familiar (genetically inherited) and the SOD1 mutations account for only about 10–20% of these cases. Unfortunately, drugs effective in the SOD1 G93A mice have failed in clinical trials, which may be attributed to differences in pathology between SOD1-driven and other types of ALS [6]. More recently, the nuclear RNA-binding proteins, called fused in sarcoma (FUS) and transactive response DNA binding protein of 43 kDa (TDP-43) have been identified in aggregates present in motor neurons of some cases of ALS [7]. In fact, TDP-43 pathology is present in nearly 95% of all cases of ALS, and has been recognized as the most common proteinopathy in both familial and sporadic cases of ALS. TDP-43 aggregates are also the hallmark of frontotemporal lobular dementia (FTLD) patients with TDP-43 inclusions (FTLD-TDP), another neurodegenerative proteinopathy [8].

In healthy neurons, TDP-43 resides mainly in the nucleus where it regulates the splicing patterns of transcripts and the expression of several important genes. In disease-affected neurons, the dynamic equilibrium of TDP-43 between nucleus and cytoplasm is altered. As a result, TDP-43 concentration increases in the cytoplasm, possibly as a mixed consequence of genetic susceptibility, aging, prolonged stress, chronic inflammation, etc. [9] The loss of TDP-43 from the nucleus prevents its normal functions, such as the regulation of RNA metabolism. While in the cytoplasm, TDP-43 experiences different post-translational modifications including truncation, ubiquitination, phosphorylation, acetylation, etc. that leads to the formation of toxic aggregates within the motor neurons, and prevents TDP-43 gene regulation activity [10]. Of these modifications, phosphorylation is the most consistent marker of pathological TDP-43 and has been implicated in its neurotoxicity. In the search for new therapeutic agents for ALS and others neurodegenerative diseases, TDP-43 emerges as a promising drug target. Restoration of TDP-43 homeostasis by using small molecules may be one of the potential approaches [11].

Protein kinases are well established drug targets, with more than forty kinase inhibitors on the market as drugs for the treatment of oncological diseases [12], and other pathologies such as rheumatoid arthritis, pulmonary fibrosis, myelofibrosis and quite recently, glaucoma [13]. Kinases, which are responsible for protein phosphorylation, are involved in many different cellular signaling events and also play crucial roles in post-translational modifications of numerous proteins. In its pathological state, TDP-43 can be phosphorylated by several kinases. These include casein kinase 1 (CK-1) delta and epsilon [14]. In fact, benzothiazole-based CK-1 inhibitors are able to decrease TDP-43 phosphorylation both in cellular and animal models [15,16]. More recently, they have been demonstrated to promote recovery of TDP-43 homeostasis, i.e. protein phosphorylation decrease and nuclear localization recovery, in human based cell models from FTLD and ALS patients [17,18]. These data indicate the promise of kinase inhibitors broadly, and CK-1 inhibitors specifically, as compounds of interest for further development as potential ALS and FTLD therapies.

Recent research has identified three additional kinases controlling TDP-43 phosphorylation *in vivo*. These are cell division cycle kinase 7 (CDC7) and tau tubulin kinase 1 and 2 (TTBK1 and

TTBK2) [19,20]. Thus, inhibitors of these kinases may be innovative drug candidates for the future effective treatment of ALS and FTLD. In fact, CDC7, a serine/threonine kinase that is essential for regulating DNA replication in all eukaryotes, has been an attractive target for cancer therapy [21]. Several inhibitors have been synthesized [22,23] and used as versatile chemical tools to decipher the role of pharmacological CDC7 inhibition in different cancer types, some of them reaching clinical trials [24]. Among them, the CDC7 inhibitor PHA-767491, that failed in clinical trial phase 1 for solid tumors, has recently shown to decrease TDP-43 phosphorylation in *C. elegans* [19] but it is not able to cross the blood brain barrier in vertebrates, and thus it is not possible to use it to study central nervous system pathologies [19]. Moreover, PHA-767491 also inhibits CDK9 [25], making it difficult to decipher the main kinase involved in its therapeutic potential over TDP-43 alteration.

Considering this back-ground, a medicinal chemistry program focused on finding selective and brain permeable small molecules CDC7 inhibitors able to modulate TDP-43 pathology was started. In the present manuscript, we describe the discovery, synthesis and optimization of a new family of selective and ATP-competitive CDC7 inhibitors based on 6-mercaptapurine scaffold. Moreover, we test their ability to reduce TDP-43 phosphorylation both in cultured cells and in two transgenic animal models of ALS. Altogether, compounds here described could be considered as new drug candidates for the future therapy of ALS and/or FTLD or as versatile tools to explore the role of CDC7 in different neurological disorders where TDP-43 is involved.

2. Results and discussion

2.1. Hit identification

A forward chemical genetic approach was used to identify new CDC7 inhibitors. This methodology has two main steps: first, identifying molecules able to interact with the target of interest and second, confirming target engagement activity in a phenotypic assay. Therefore, we first selected an *in vitro* biological assay to evaluate CDC7 activity [26]. A set of chemically diverse compounds were chosen from our in-house MBC chemical library, which has been recognized as a valuable tool to provide drug-like hit molecules for screening [27]. We initially assayed the potential inhibition of CDC7 by each of these molecules at a fixed concentration of 10 μ M. For compounds where the percentage of kinase inhibition was greater than the 50%, a dose-response curve was calculated and the IC₅₀ value determined. Following this approach, the benzoylmercaptapurine derivative **1** was identified with an IC₅₀ value of 2.12 μ M emerging as a new chemical prototype for CDC7 inhibition (Fig. 1).

2.2. Hit optimization. Chemical synthesis

A medicinal chemistry program was then designed to produce a

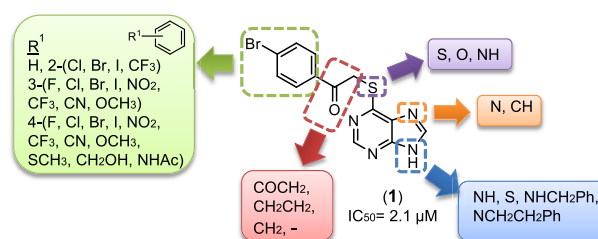


Fig. 1. Chemical structure of the new CDC7 inhibitor identified, benzoylmercaptapurine **1**, and chemical modifications proposed.

focused set of compounds with different structural modifications around the central heterocyclic scaffold, allowing us to study the influence of different substituents in CDC7 inhibition (Fig. 1). Using different synthetic strategies previously described, a set of more than 30 compounds was synthesized, purified and characterized. Changes in the nature of heteroatoms, the nature and length of the linker joined to the mercaptopurine core, the nature and position of substituents in the phenyl ring have been made to optimize the biological potency of the hit compound building a consistent structure-activity relationship.

Initially, substituents in the phenyl ring of the benzoyl-mercaptopurine derivative **1** were varied using 6-mercaptopurine and different bromoacetophenones as reagents. In that case, nucleophilic substitution in basic aprotic medium yielded derivatives **1–3**. The same reaction conditions were applied to obtain 6-benzylmercaptopurines (**4–25**), where the carbonyl group is eliminated from the linker, and 6-phenethylmercaptopurines (compounds **26–29**) where the carbonyl group is substituted by a methylene group. Many diverse benzylhalides were used as reagents in basic medium and in some cases a mixture of two compounds was obtained that after isolation provided the 6-benzylmercaptopurines substituted at N-9 as minority compound (**7b**, **15b**, **23b–25b**). When phenethylhalides were used, disubstituted derivatives (**26b–29b**) were isolated every time (Scheme 1).

Derivatives without any spacer between the sulfur atom of the mercaptopurine-central core and the phenyl substituent were obtained by aromatic nucleophilic substitution of 6-chloropurine with different thiophenols under basic catalysis in *n*-butanol. Compounds **30** and **31** were isolated in good yields. The aromatic nucleophilic substitution using different benzyl alcohols or benzylamines in basic medium or under microwave irradiation respectively was also used to yield substituted oxo- and aminopurines, derivatives **32–35**, where the sulfur atom of the hit **1** is replaced by its bioisosters such as nitrogen or oxygen ones (Scheme 2).

Finally, modifications of the heterocyclic core were proposed and 7*H*-pyrrolo[2,3-*d*]pyrimidines and thieno[2,3-*d*]pyrimidines (compounds **36–39**) were synthesized by nucleophilic substitution of the chlorine atom of 4-chloro-7*H*-pyrrolo[2,3-*d*]pyrimidine or 4-

chlorothieno[2,3-*d*]pyrimidine with the appropriate benzyl mercaptane derivative in basic polar aprotic medium (Scheme 2).

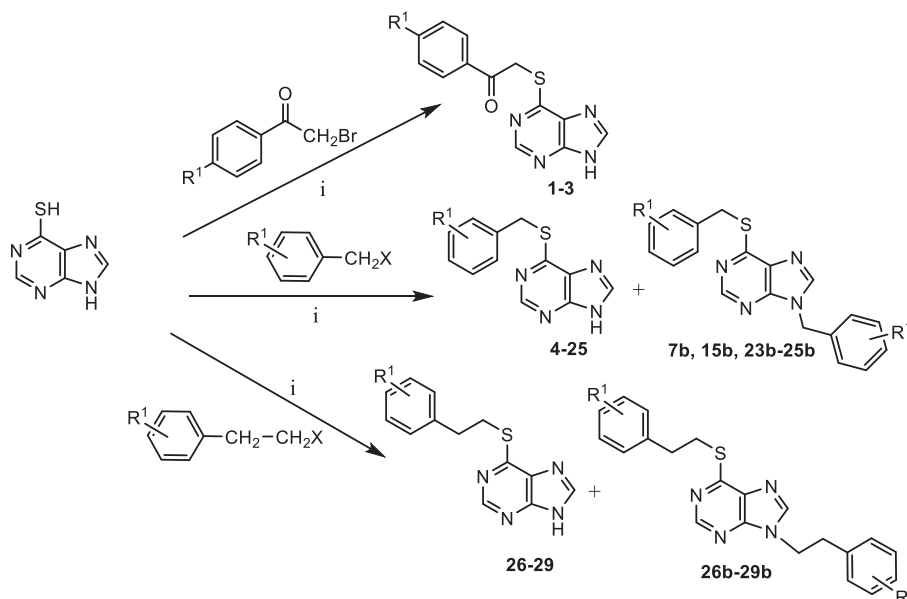
Although some of the compounds were previously described, we fully characterized here the structures of all the synthesized compounds unequivocally based on their spectroscopical (¹H and ¹³C NMR) and analytical data. They are collected in the experimental part and supporting information.

2.3. Biological evaluation of CDC7 inhibition

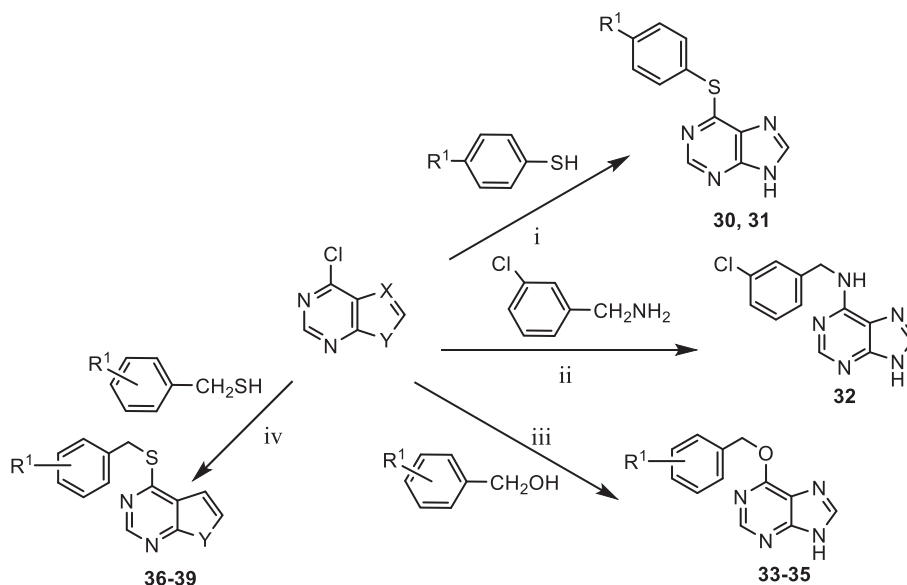
The purine-based prepared heterocyclic derivatives (**2–39**) were evaluated in a commercially available CDC7 activity assay to determine their potential inhibition. CDC7 is only active when it is associated with its activation unit Dbf4, and interaction with Dbf4 is necessary for CDC7 ATP recognition and substrate binding [28]. Thus, the methodology utilizes a fluorescein-labeled substrate of CDC7/Dbf4 and an associated specific antibody, which results in an increased TR-FRET value when this substrate and ATP are allowed to react. The amount of antibody that is bound to the tracer is directly proportional to the amount of phosphorylated substrate present and in this manner, kinase activity can be detected and measured by an increase in the TR-FRET value. All the compounds were initially tested at a fixed concentration of 10 μM and the IC₅₀ was calculated when the percentage of inhibition was greater than 50%. Results are collected in Table 1 showing a large collection of CDC7 inhibitors with IC₅₀ values in the submicromolar range, more potent than the initial hit **1**. For comparative purposes, the well-known CDC7 inhibitor called PHA-767491 is also included in Table 1 as standard reference.

In view of the results collected in Table 1, some preliminary structure-activity relationships could be established. Firstly, the presence of the heterocyclic NH in the imidazole-fused ring is crucial for activity and totally inactive compounds are obtained when any substituent is attached to this nitrogen atom such is the case of compounds **7b**, **15b**, and **23b–29b** or when this NH is replaced by a sulfur atom (thieno[2,3-*d*]pyrimidines **36** and **37**).

The length and the nature of the linker attached to the exocyclic sulfur atom also influence the potency of CDC7 inhibition. While kinase inhibition is similar in mercaptopurines **1–3**, in the



Scheme 1. I) K₂CO₃, DMF, r. t.



Scheme 2. i) Et_3N , K_2CO_3 , $n\text{-BuOH}$, reflux; ii) MW, $100\text{ }^\circ\text{C}$, 5 min; iii) NaOH , reflux; iv) NaH , DMF , r. t.

micromolar range, it increases one order of magnitude when the carbonyl group is eliminated from the spacer between both of the aromatic fragments (derivatives **4–6**). However, CDC7 inhibition decreases when the linker disappears and the phenyl moiety is directly attached to the sulfur atom of mercaptopurine scaffold (compounds **30** and **31**). It is important to note that inhibitory potency also increases when the carbonyl group present in the linker of the hit compound **1** is changed to a methylene group (purines derivatives **26–29**).

Finally, it is worthwhile to mention that the exocyclic sulfur atom may be replaced by its bioisostere, the oxygen atom (compounds **15** and **7** versus **33** and **34**, respectively) without affecting the kinase inhibition, but the inhibitory potency significantly decreases when the sulfur is substituted by an NH group (derivative **32**).

In general, the nature and the substitution position of different groups in the phenyl ring do not seriously affect the inhibition of CDC7 by this family of mercaptopurines, having a great number of compounds (derivatives **4–25**) with IC_{50} values in the sub-micromolar range, between 0.1 and 0.9 μM .

To study the binding mode of these new CDC7 inhibitors, the kinetic mechanism of CDC7 inhibition was investigated by varying the concentrations of both ATP and the tested inhibitors in the kinase reaction. Three of the most potent compounds and firstly available, derivatives **7**, **15** and **22** were selected for this assay with the goal of extrapolating the result to all the purine-based CDC7 inhibitors here described. For this goal, we chose a substrate phosphorylating assay based on ADP-Glo™ technology checking the previous inhibitory activity found. The Lineweaver-Burk or double-reciprocal plots of $1/v$ versus $1/[\text{ATP}]$ at fixed concentrations of these selected inhibitors showed an intersecting pattern consistent with an ATP-competitive inhibition as all lines converge at or near the y axis (Fig. 2). These results show that mercaptopurine-based derivatives, and specifically compounds **7**, **15** and **22**, are ATP competitive CDC7 inhibitors.

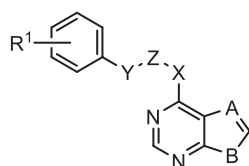
As there is conservation between ATP binding sites among the kinome, kinase inhibitors targeting the ATP binding site may have a lack of selectivity and potential undesirable side effects precluding further drug development. To start the assessment of kinase selectivity in this new family of compounds, the three previous

selected compounds were tested against a limited set of kinases based on structural assessment. In all cases, compounds were tested at 10 μM in forty-three CDC7 structurally related kinases such as cyclin dependent kinases (CDKs), proto-oncogene serine/threonine-protein kinases (PIMs), casein kinases (CSNKs) and dual specificity tyrosine-phosphorylation-regulated kinases (DYRKs). The three compounds tested were very selective in the kinase panel evaluated, as no special potent inhibition was observed for the evaluated kinases besides CDC7 (Fig. 3). The final selectivity score or “S” score, a quantitative measure of compound selectivity calculated by dividing the number of kinases that compounds bind to by the total number of distinct kinases tested [29], is 0.023 for the three compounds as they only interact with 1 out of 43 kinases evaluated with a percentage of activity below 5%. These data point to a selective new family of CDC7 inhibitors despite being ATP-competitive.

2.4. *In silico* binding mode studies

The high degree of kinase selectivity of our purine-based inhibitor for CDC7 compared to structurally similar kinases such as casein kinase family members, led us to explore their potential binding mode by computational techniques. In fact, CDC7 has unique features in its structure with respect to other kinases [30]. To gain insights into the interaction between CDC7 and the purine derivatives here described, a molecular modeling study was performed using the published crystal structure of the CDC7 kinase in complex with PHA-767491 (PHA) (PDB entry: 4F9B) [31]. All purine derivatives with an IC_{50} below 10 μM were docked into the ATP-binding site of the protein using Glide software (see Experimental Section) based in our experimental ATP competition results. To assess the reliability of the results, the same docking protocol was applied to adenosine diphosphate (ADP) and PHA, the known CDC7 inhibitor, both crystallized into the protein. No differences with the X-ray experimental complex (Fig. S1) were shown, validating the docking procedure. Then, MM-GBSA calculations were performed to postprocess and re-score the ligand docking solutions and to correlate their structural binding mode with the experimental activity against CDC7. The predicted binding free energies values (ΔG_{bind}) against the experimental activities (pIC_{50}) reveal a

Table 1
CDC-7 inhibition and BBB permeability prediction of synthesized mercaptopurine derivatives (**1–35**) and heterocyclic analogues (**36–39**).



Comp. No.	A	X	Z	Y	R ¹	B	CDC-7 IC ₅₀ (μM) ^{a,b}	BBB Prediction
1	N	S	CH ₂	C=O	p-Br	NH	2.12 ± 1.50	n.t.
2	N	S	CH ₂	C=O	p-Cl	NH	4.15 ± 2.64	n.t.
3	N	S	CH ₂	C=O	p-NO ₂	NH	3.11 ± 1.68	n.t.
4	N	S	CH ₂	—	p-Br	NH	0.44 ± 0.11	CNS +
5	N	S	CH ₂	—	p-Cl	NH	0.18 ± 0.08	CNS +
6	N	S	CH ₂	—	p-NO ₂	NH	0.13 ± 0.01	CNS +
7	N	S	CH ₂	—	H	NH	0.20 ± 0.04	CNS +
7b	N	S	CH ₂	—	H	NCH ₂ Ph	0% ^c	n.t.
8	N	S	CH ₂	—	p-I	NH	0.30 ± 0.03	CNS +
9	N	S	CH ₂	—	p-CF ₃	NH	0.36 ± 0.07	CNS +
10	N	S	CH ₂	—	p-CN	NH	0.29 ± 0.07	CNS+/CNS-
11	N	S	CH ₂	—	p-SMe	NH	0.14 ± 0.01	CNS +
12	N	S	CH ₂	—	p-NHAc	NH	0.47 ± 0.06	CNS -
13	N	S	CH ₂	—	p-CH ₂ OH	NH	0.30 ± 0.02	CNS+/CNS-
14	N	S	CH ₂	—	m-Br	NH	0.13 ± 0.03	CNS -
15	N	S	CH ₂	—	m-Cl	NH	0.14 ± 0.03	CNS +
15b	N	S	CH ₂	—	m-Cl	NCH ₂ (3ClPh)	30% ^c	n.t.
16	N	S	CH ₂	—	m-NO ₂	NH	0.19 ± 0.03	CNS+/CNS-
17	N	S	CH ₂	—	m-I	NH	0.08 ± 0.02	CNS +
18	N	S	CH ₂	—	m-CF ₃	NH	0.32 ± 0.06	CNS +
19	N	S	CH ₂	—	m-CN	NH	0.34 ± 0.06	CNS+/CNS-
20	N	S	CH ₂	—	m-OMe	NH	0.24 ± 0.06	CNS +
21	N	S	CH ₂	—	m-F	NH	0.36 ± 0.05	CNS +
22	N	S	CH ₂	—	o-Br	NH	0.27 ± 0.06	CNS +
23	N	S	CH ₂	—	o-Cl	NH	0.09 ± 0.02	CNS +
23b	N	S	CH ₂	—	o-Cl	NCH ₂ (2ClPh)	7% ^c	n.t.
24	N	S	CH ₂	—	o-I	NH	0.58 ± 0.10	CNS +
24b	N	S	CH ₂	—	o-I	NCH ₂ (2 IPh)	4% ^a	n.t.
25	N	S	CH ₂	—	o-CF ₃	NH	0.25 ± 0.07	CNS +
25b	N	S	CH ₂	—	o-CF ₃	NCH ₂ (2CF ₃ Ph)	9% ^c	n.t.
26	N	S	CH ₂	CH ₂	p-Cl	NH	0.14 ± 0.03	CNS +
26b	N	S	CH ₂	CH ₂	p-Cl	N(CH ₂) ₂ (4ClPh)	3% ^c	n.t.
27	N	S	CH ₂	CH ₂	p-F	NH	0.39 ± 0.05	CNS +
27b	N	S	CH ₂	CH ₂	p-F	N(CH ₂) ₂ (4FPh)	12% ^c	n.t.
28	N	S	CH ₂	CH ₂	m-Cl	NH	0.30 ± 0.04	CNS +
28b	N	S	CH ₂	CH ₂	m-Cl	N(CH ₂) ₂ (3ClPh)	8% ^c	n.t.
29	N	S	CH ₂	CH ₂	o-Cl	NH	0.19 ± 0.03	CNS +
29b	N	S	CH ₂	CH ₂	o-Cl	N(CH ₂) ₂ (2ClPh)	4% ^c	n.t.
30	N	S	—	—	p-Br	NH	1.38 ± 0.43	n.t.
31	N	S	—	—	p-OMe	NH	1.72 ± 0.26	n.t.
32	N	NH	CH ₂	—	m-Cl	NH	3.06 ± 1.00	n.t.
33	N	O	CH ₂	—	m-Cl	NH	0.19 ± 0.05	CNS +
34	N	O	CH ₂	—	H	NH	0.17 ± 0.04	CNS+/CNS-
35	N	O	CH ₂	—	p-Br	NH	0.91 ± 0.24	CNS +
36	CH	S	CH ₂	—	H	S	18% ^c	n.t.
37	CH	S	CH ₂	—	m-Br	S	11% ^c	n.t.
38	CH	S	CH ₂	—	H	NH	0.23 ± 0.04	CNS +
39	CH	S	CH ₂	—	m-Br	NH	0.39 ± 0.11	n.d.

n.t. = not tested; n.d.: not possible to determine in the experimental conditions.

^a Reference compound PHA-767491: IC₅₀ = 0.01 μM.

^b IC₅₀ Values ± Standard deviation (ten different concentrations per compound, in two independent experiments) Origin 9.0 software used.

^c This value represents the % of CDC7 inhibition at a fix compound concentration of 10 μM.

moderate relationship between these two variables (correlation coefficient $R^2 = 0.72$) (Fig. S2). The ΔG_{bind} values for CDC7 inhibitors vary between -49.57 and -41.41 kcal/mol. This computational protocol (docking + MM-GBSA) has been successfully used to study correlations between theoretical affinities and experimental activities [32,33], and here we used it to further study the structure-activity relationship of thirty four different purine derivatives against CDC7. In this way, compounds **2**, **15**, **26**, **30**, **32**, and **33** were

selected in order to explore the effect of the nature and the length of the linker in CDC7 inhibition.

Computational analysis suggests that there are two key interactions for the activity of the new CDC7 inhibitors: two hydrogen bonds between the purine central core and Pro135 and Leu 137 (Fig. 4). The lack of one of these two interactions is translated in a loss of the activity confirming the experimental results obtained for purines *N*-substituted such as **7b**, **15b**, and **23b-29b** or thieno[2,3-

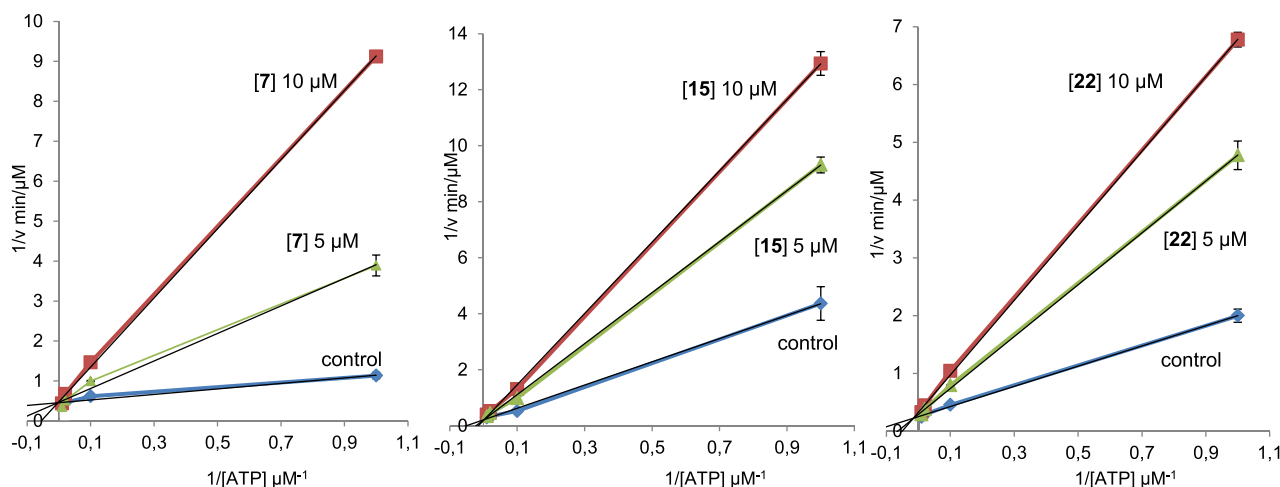


Fig. 2. Kinetic data determined for derivatives **7**, **15** and **22**. ATP concentrations in the reaction mixture varied from 1 to 100 μM . Compound concentrations used are depicted in the plot and the concentration of the substrate was kept constant at 12.5 μM . Each point is the mean of two different experiments, each one analyzed in duplicate.

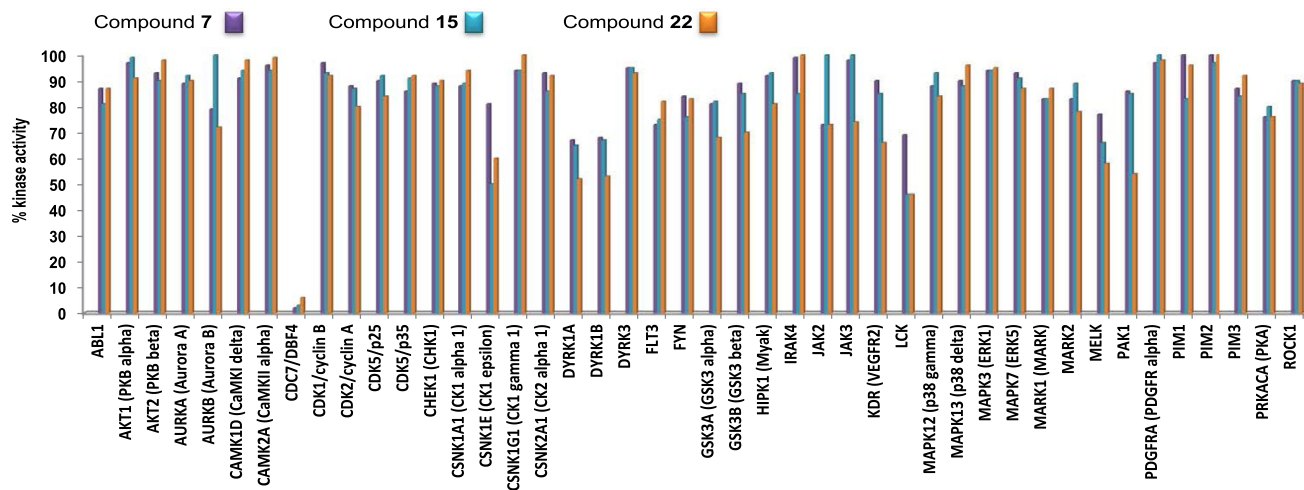


Fig. 3. Kinase profiling for CDC7 inhibitors **7**, **15** and **22**.

d]pyrimidines **36** and **37**, all of them inactive compounds.

Among active compounds, the computational study has allowed us to rationalize the relationship between the chemical structure and biological activity. Regarding the length of the linker between the purine moiety and the phenyl ring, the activity increases when the carbonyl group is suppressed (i.e. compound **15**). In contrast, the activity of the inhibitors decreases when linker disappears and the phenyl moiety is directly bonded to the sulfur atom (i.e. compound **30**). The reason could be that the phenyl moiety in **15** make more extensive van der Waals contacts with the catalytic residues Lys90, Asp196, Ser 181 and Asn 182 [30]. In fact, a clear π -cation interaction between compound **15** and Lys90 stabilizes the binding of this compound. In contrast, the less potent compound **30** interacts with His139 through a π - π stacking interaction, being less exposed to other important residues as mentioned above.

Considering the linker nature, the activity of purine-based CDC7 inhibitors increases when a methylene moiety substitutes the carbonyl group (i.e. compound **26** vs **2**). This difference in the biological activity can be explained by analyzing the components of the ΔG_{bind} energy calculated by MM-GBSA (Table 2). Compounds **15** and **26** have similar binding energies, with relative ΔG_{bind}

between -48 and -49 kcal/mol. However, compound **2** has a relative $\Delta G_{\text{bind}} = -42$ kcal/mol. The major difference in the binding energies of these compounds lies in the polar contribution of the solvation energy (ΔG_{GB}) where compound **2** presents a difference of 6.5 kcal/mol in comparison with compounds **15** and **26**. Although this difference is not so significant, it makes the molecule **2** more difficult to be desolvated prior to enter in the binding site. In this way, the carbonyl group of the molecule **2** locates in the outer part of the cavity, being more exposed to the solvent (Fig. 4).

Regarding the heteroatom of the linker, when the sulfur (compound **15**) is replaced by an oxygen (compound **33**), the activity as well as the ΔG_{bind} does not change. However, when it is replaced by an amine group (compound **32**), both CDC7 inhibition activity and relative ΔG_{bind} decreases. This variation may be also explained by analyzing the components of the ΔG_{bind} energy. Compound **15** has a relative ΔG_{bind} of -48 kcal/mol, while compound **32** has a relative $\Delta G_{\text{bind}} = -41$ kcal/mol. The major difference between these two compounds lies in the van der Waals interaction energy, 8 kcal/mol between them (Table 2).

Finally, it is worth mentioning that the main deviation in the binding mode of purine-based CDC7 inhibitors compared to the

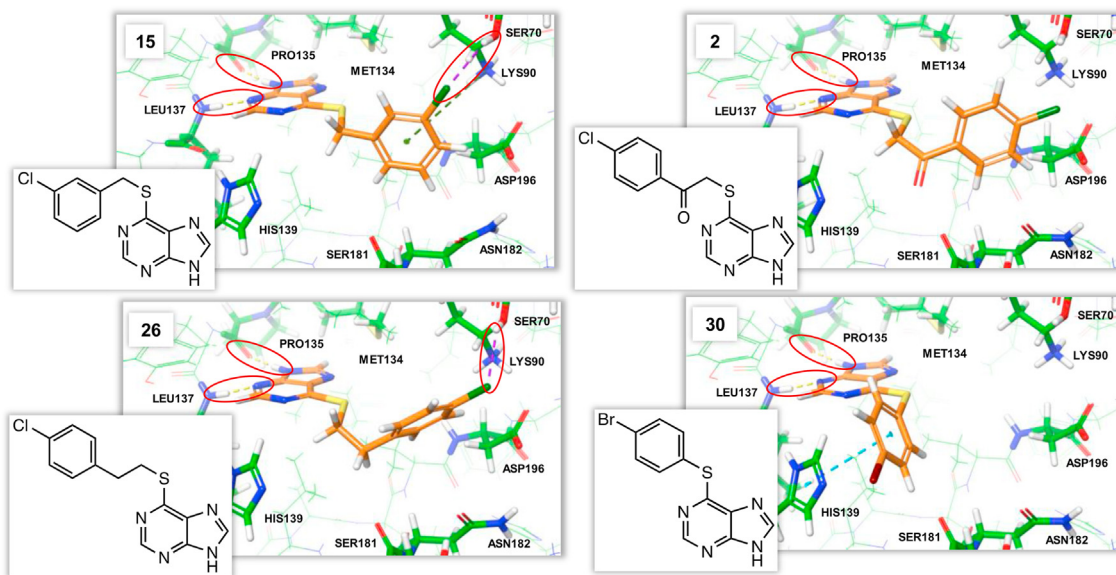


Fig. 4. Binding modes of compound **15** vs. **2**, **26**, and **30** in the catalytic site of CDC7.

Table 2

Binding energies (kcal/mol) calculated by MM-GBSA of compounds **2**, **15**, **26**, **30**, **32** and **33**.

Comp.	IC ₅₀ (μ M)	ΔG_{bind}	ΔE_{MM}					ΔG_{sol}			
			$\Delta E_{\text{internal}}^a$	Hbond _{cor} ^a	Packing _{cor} ^a	SelfCont _{cor} ^a	$\Delta E_{\text{Coulomb}}^a$	ΔE_{vdW}^a	ΔG_{GB}^a	ΔG_{SA}^a	
2	4.15	-42.27	4.332	-0.334	-0.172	0.003	-24.424	-41.48	29.83	-10.03	
15	0.14	-48.04	1.369	0.102	-0.810	0.299	-24.221	-37.62	23.39	-10.55	
26	0.14	-49.57	3.030	-0.703	-0.703	0.012	-24.942	-39.09	23.32	-10.58	
30	1.38	-45.01	-0.044	-0.613	-0.613	0.008	-25.036	-31.76	21.94	-8.82	
32	3.06	-41.65	1.249	-0.499	-0.499	0.116	-26.940	-29.71	23.99	-9.67	
33	0.19	-48.71	0.185	-0.607	-0.607	0.055	-24.844	-33.13	19.05	-9.17	

^a Contribution to the total energy from different components: $\Delta E_{\text{internal}}$ = Covalent binding energy; Hbond_{cor} = Hydrogen-bonding correction; Packing_{cor} = π - π packing correction; SelfCont_{cor} = Self-contact correction; $\Delta E_{\text{Coulomb}}$ = Coulomb energy; ΔE_{vdW} = van der Waals energy; ΔG_{GB} = Generalized Born electrostatic solvation energy; ΔG_{SA} = Lipophilic energy.

well-characterized PHA is the presence of a hydrogen-bond interaction in the hinge region between the backbone carbonyl group of Pro135 and the heterocyclic NH and, the lack of H-bonding with catalytic residues such as Lys90 or Asp196 (Fig. 4 and S1). Therefore, PHA binds not only to CDC7 but also to different structural related kinases such as CDK1 and CDK2 [34], being a dual inhibitor of CDK9 [35]. Somehow, the new described purine-based compounds, less potent but much more selective than PHA inhibitor, point to a new well-conserved binding mode that gives new hints for further potency improvements. One of the main reasons that can explain this selectivity may be that purine-based compounds here described form van der Waals contacts with Ser70, Met 118 and His139 which are some of the most variable residues among protein kinases. Even more, compounds **15** and **26** present halogen bond interactions with Ser70 (Fig. 4).

2.5. Blood brain barrier (BBB) permeability

Brain penetrant chemical probes and/or drug candidates are needed when a central nervous system disease, such as ALS, is going to be studied in animal models. Here, we have used a parallel artificial membrane permeability assay (PAMPA) using porcine lipid to emulate the human blood brain barrier (BBB) in order to determine this essential drug-like characteristic for our compounds of interest. We calculated the predicted brain permeability for all the compounds with an IC₅₀ value for CDC7 inhibition below 1 μ M. In

this assay, ten reference commercial drugs used clinically with known brain permeability are included as controls. A good correlation between experimental-described values was obtained $Pe(\text{exptl}) = 0.849(\text{bibl}) - 0.1282(R^2 = 0.9828)$ (Fig. S3). From this equation and following the pattern established in the literature for BBB permeation prediction [36] we could classify compounds as CNS + when they present a permeability $> 3.26 \times 10^{-6} \text{ cm s}^{-1}$. Based on these results we can consider that a large number of compounds, specifically **4–9**, **11**, **15**, **17**, **18**, **20–29**, **33**, **35**, and **38**, are predicted to be able to cross the BBB by passive permeation (Fig. 5, Table 1 and Table S3) and thus they can be considered for further pharmacological studies in neurological diseases. Compounds **10**, **13**, **16**, **19**, and **34** are borderline for PAMPA permeability (CNS+/CNS-), and finally compounds **12** and **14** are predicted to not be able to cross the BBB (CNS-). Compound **39** precipitates under the experimental conditions employed; therefore, there was not a clear UV spectrum after filtration making it impossible to determine the BBB permeability.

2.6. TDP-43 modulation by CDC7 inhibitors in cellular and in vivo models

2.6.1. Neuroprotective effect of CDC7 inhibitors in a neuronal cell model of induced TDP-43 phosphorylation by ethacrynic acid treatment

The next step was to determine if small molecule inhibition of

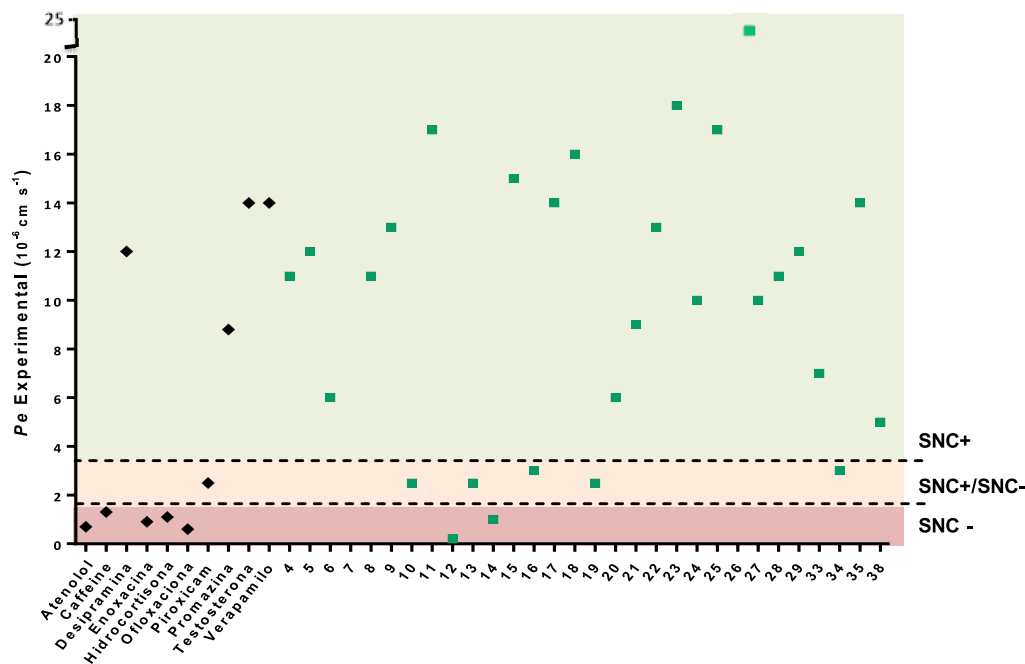


Fig. 5. PAMPA *in vitro* permeability (P_e) plot of CDC7 inhibitors (green squares) and control drugs (black diamonds). CNS + (green) for compounds with $P_e > 3.26 \times 10^{-6} \text{ cm s}^{-1}$, CNS- (red) for $P_e < 1.56 \times 10^{-6} \text{ cm s}^{-1}$ and CNS+/SNC- (orange) for $1.56 \times 10^{-6} < P_e < 3.26 \times 10^{-6} \text{ cm s}^{-1}$. Data represent the mean \pm SD from two independent experiments. (For interpretation of the references to colour in this figure legend, the reader is referred to the Web version of this article.)

CDC7 kinase activity, by the new purine-based inhibitors may prevent TDP-43 phosphorylation *in vitro*. In order to be sure that results of interest are produced by CDC7 inhibition, we tested a large set of 23 compounds with brain permeability values compatible with the ability to cross the BBB. The selected cell model was a neuronal cell-based model of induced TDP-43 phosphorylation driven by glutathione depletion. Human neuroblastoma cell line SH-SY5Y cells were pre-treated with CDC7 inhibitors for 1 h and phosphorylation of endogenous cellular TDP-43 was then induced with exposure to ethacrynic acid (EA) for 24 h [37]. Compound dose was selected as 10 μM after evaluating cell viability in the presence or absence of CDC7 inhibitors at 5 and 10 μM in SH-SY5Y (Fig. S4). As seen in Fig. 6, the addition of EA to the SH-SY5Y cells resulted in significant cell death, which is partially prevented by several of the CDC7 inhibitors treatment. As reference control, we used tideglusib, a GSK-3 inhibitor with neuroprotective activity by decreasing TDP-43 phosphorylation.

To check if the neuroprotective effect of CDC7 inhibitors is produced by a decrease in TDP-43 phosphorylation state, Western-blot analysis was done using a phospho-specific (S409/410) anti-TDP-43 antibody. In Fig. 7 the increase of TDP-43 phosphorylation caused by EA is shown together with the reduction of this aberrant phosphorylation produced with the CDC7 inhibitors treatment. CDC7 inhibitors had no effect on total cellular levels of TDP-43.

Furthermore, to fully check whether the inhibition of TDP-43 phosphorylation here reported in SH-SY5Y by CDC7 inhibitors treatment reduces the amount of TDP-43 cytoplasmic localization, an immunofluorescence analysis was performed with derivative 15. Results depicted in Fig. 8 showed the decreased of cytosolic TDP-43 after the treatment with the CDC7 inhibitor 15, which is in agreement with previous results [17]. Moreover, two of the compounds described here, derivatives 7 and 15, have been proved to be capable to restore the normal nuclear TDP-43 levels in immortalized lymphocytes derived from either sporadic ALS or FTLD-TDP

patients [38].

Taken together, these results may point to CDC7 inhibition as a potential viable strategy to reduce neurotoxic TDP-43 phosphorylation and cellular localization.

2.7. CDC7 inhibitor testing in transgenic *C. elegans*

In order to determine whether inhibition of CDC7 kinase activity by novel CDC7 inhibitors will prevent TDP-43 phosphorylation *in vivo*, we utilized as a starting point transgenic *Caenorhabditis elegans* expressing human familial ALS mutant TDP-43 pan-neuronally (TDP-43 tg) [39]. *C. elegans* are a tractable invertebrate animal for studying neurodegenerative disease, as they have a well-characterized differentiated nervous system that includes the major neuronal types found in humans [40]. TDP-43 tg *C. elegans* exhibit age-dependent motor dysfunction, progressive neurodegeneration, and accumulate robust amounts of phosphorylated TDP-43 [39]. The *C. elegans* cuticle is a highly impervious barrier that prevents many small molecules from entering [41]; therefore, the concentration of small molecule required to see an effect in *C. elegans* is typically high and may not reflect the effective dose that penetrates into the body of the animals [42]. However, despite these limitations, *C. elegans* have been successfully used to demonstrate *in vivo* activity of small molecules including kinase inhibitors [19,43]. To assay CDC7 inhibitors in *C. elegans*, TDP-43 tg animals were raised on solid media in the presence of the CDC7 inhibitors, grown for 6 days, and harvested for immunoblot analysis. We tested the well characterized purine-based CDC7 inhibitors 7, 15 and 22 and found that levels of phosphorylated TDP-43 were significantly reduced following treatment with inhibitor 7, with no apparent effect on total levels of TDP-43 (Fig. 9). Compounds 15 and 22 had more variable effects on TDP-43 phosphorylation, which may be a consequence of a differential ability to effectively cross through the cuticle of *C. elegans*. Nevertheless, we show that

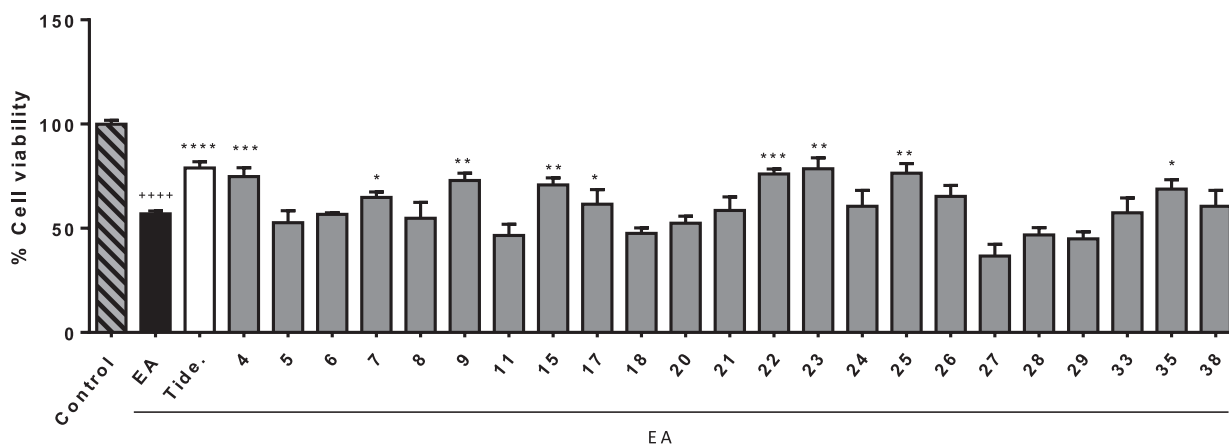


Fig. 6. Neuroprotective effect of CDC7 inhibitors at a fixed concentration of 10 μ M in neuroblastoma SH-SY5Y cells after being exposed to 20 μ M of EA for 24 h. Commercial GSK-3 β inhibitor (Tideglusib 5 μ M) was used as internal control. Cell viability was measured by MTT assay. Data represent the mean \pm SEM of 5 different experiments (* p < 0.05, ** p < 0.01, *** p < 0.001, **** p < 0.0001 significantly different from SH-SY5Y EA-treated cells, +++++ p < 0.0001 significantly different from Control).

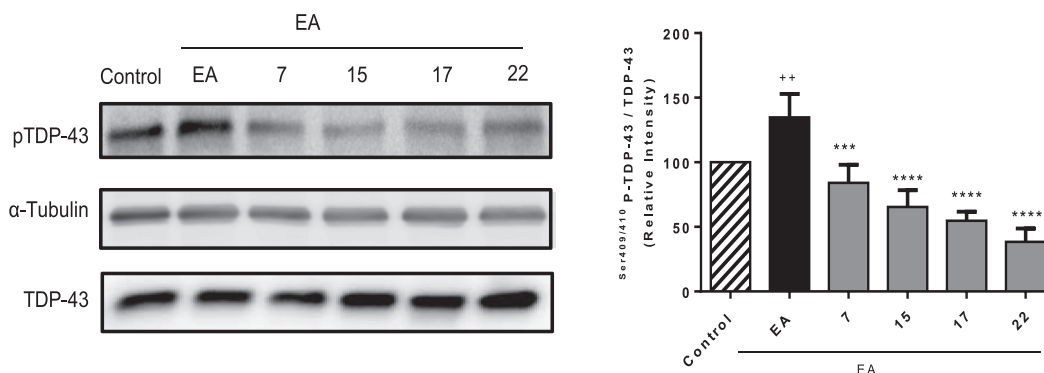


Fig. 7. Effects of CDC7 inhibitors on TDP-43 phosphorylation in neuroblastoma SH-SY5Y cells after being exposed to EA. Representative immunoblots showing pTDP-43 protein levels. Cells were exposed to EA (20 μ M) for 24 h in the presence or absence of CDC7 inhibitors (10 μ M). Data represent the mean \pm SEM of 3 different experiments. (*** p < 0.001, **** p < 0.0001 significantly different from SH-SY5Y EA-treated cells, ++ p < 0.01 significantly different from Control).

compound **7** is able to reduce TDP-43 phosphorylation *in vivo*.

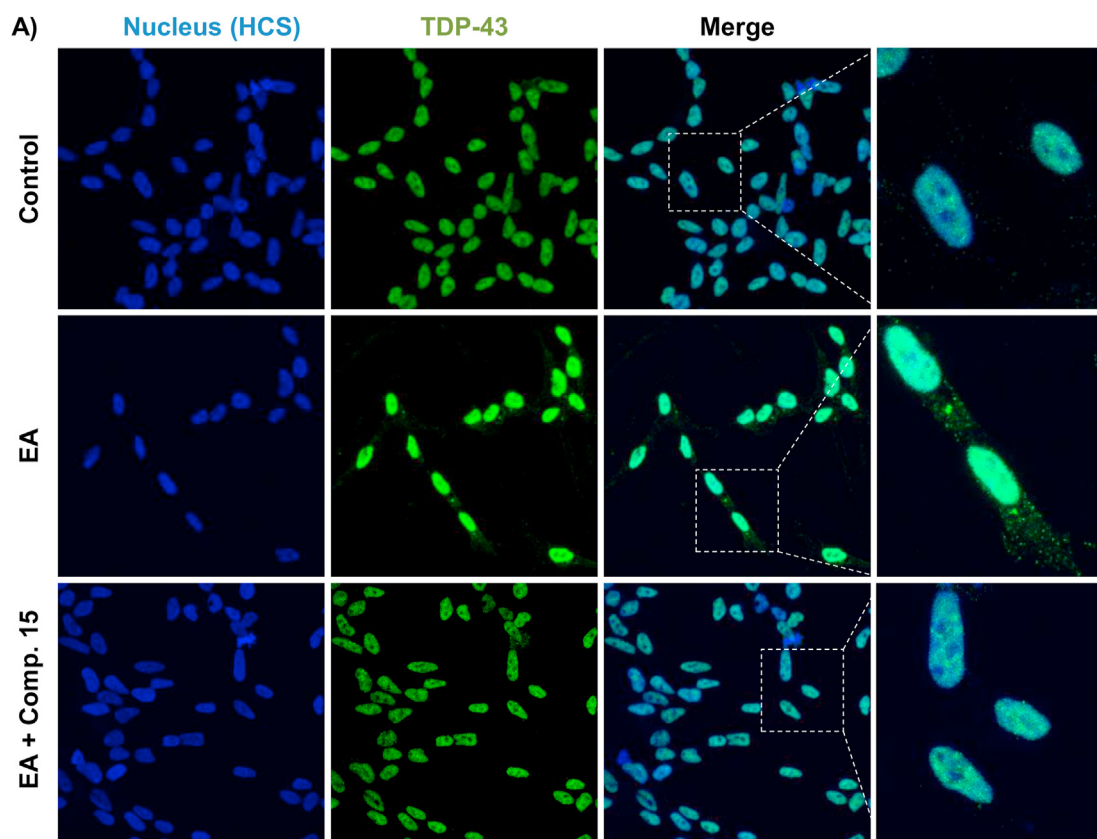
2.7.1. Treatment of TDP-43 (A315T) transgenic mice model with a CDC7 inhibitor

The encouraging obtained results prompted us to test the mercaptopurine-based CDC7 inhibitor **22** to a mouse model of ALS, following our working hypothesis that *in vivo* modulation of TDP-43 proteinopathy by CDC7 inhibitors may be a new therapeutic approach for ALS. Selection of compound **22** was done based in efficacy shown decreasing TDP-43 phosphorylation in human cell line (Fig. 7).

We have used the TDP-43 (A315T) transgenic mice, which is one of the first experimental models of ALS based on mutations in TDP-43 protein [44]. The transgene, driven by mouse prion promoter, is expressed in all neurons and glia in the spinal cord. Due to TDP-43 overexpression, transgenic mice develop motor neuron disease. We designed a chronic treatment in which compound **22** was administered intraperitoneally once a day for 30 days. Four groups each with 8 animals were studied: wild type + vehicle, wild type + compound **22**, transgenic + vehicle and transgenic + compound **22**. The trial was started with males of 65 days old. Weight was daily logged and no toxicity was observed

across the experiment (Fig. S5). Behavioral tests such as rotarod and hindlimb clasp test were weekly performed to evaluate motor coordination and muscle strength in the animals. An amelioration in the disease progression and muscle impairment was observed in the treated group in both tests (Fig. 10). Both tests measure pathological symptoms, such as muscle weakness, balance disturbance and spasticity, that resemble those present during the human disease. The treatment with the CDC7 inhibitor was highly effective in attenuating clasp behavior present in TDP-43 (A315T) mice from the third week of treatment onwards (Fig. 10B). Additionally, the treatment with compound **22** produced a recovery in rotarod performance after five weeks of treatment (Fig. 10C). CDC7 inhibition had no effects in wild type animals, as measured during rotarod and hindlimb clasp tests (Fig. 10B and C).

Moreover, after Western-blot analysis in the spinal cord tissue of TDP-43 (A315T) mice, we observed a decrease in *p*-TDP-43 (Fig. 11). These results show that compound **22** is able to *in vivo* penetrate in the central nervous system confirming previous PAMPA predictions and, thus, it is able to delay the muscle strength deterioration produced in these TDP-43 (A315T) transgenic mice when it is measured by rotarod and hindlimb clasp test. Finally, all these data correlate with *in vivo* decrease of TDP-43 phosphorylation in



B)

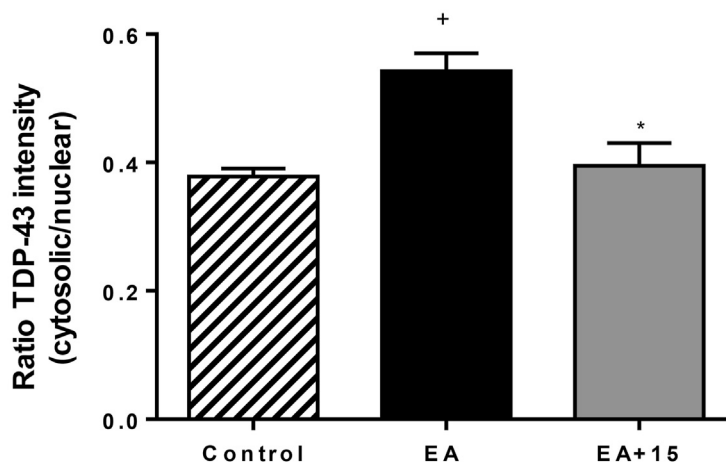


Fig. 8. Subcellular localization of TDP-43 detected by immunofluorescence after compound **15** treatment in ethacrynic acid treated SH-SY5Y cells. (A) Cells were exposed to EA (20 μ M) in the presence or absence of compound **15** (10 μ M) for 24 h. TDP-43 localization was assessed by confocal laser scanning microscopy. (B) Quantification of fluorescence intensity of TDP-43 inside and outside the nucleus was determine in at least 30 different cells from 3 separate fields. Data represent the mean \pm SEM (magnification 63 \times). (* p < 0.5 significantly different from SH-SY5Y EA-treated cells, ⁺ p < 0.05 significantly different from Control).

spinal cord after the treatment with the CDC7 inhibitor.

3. Conclusions

CDC7, a kinase involved in different oncologic processes, has emerged as a new target for different neurological conditions where the nuclear protein TDP-43 is involved including ALS, FTL and other rare diseases such as Alexander's or Pick's diseases [9]. Recently, a new Alzheimer's-like dementia disorder has been

described characterized by pathological TDP-43 and termed LATE (Limbic-predominant age-related TDP-43 encephalopathy) [45]. In this context, prevention of TDP-43 phosphorylation through the design and development of brain-permeable selective CDC7 inhibitors emerges as a potential therapeutic strategy for these severe and unmet diseases. In this manuscript we have discovered, using a chemical genetic approach, a new compound able to target CDC7. After a hit-to-lead optimization process, a family of small molecules with a central purine core was obtained as completely new CDC7

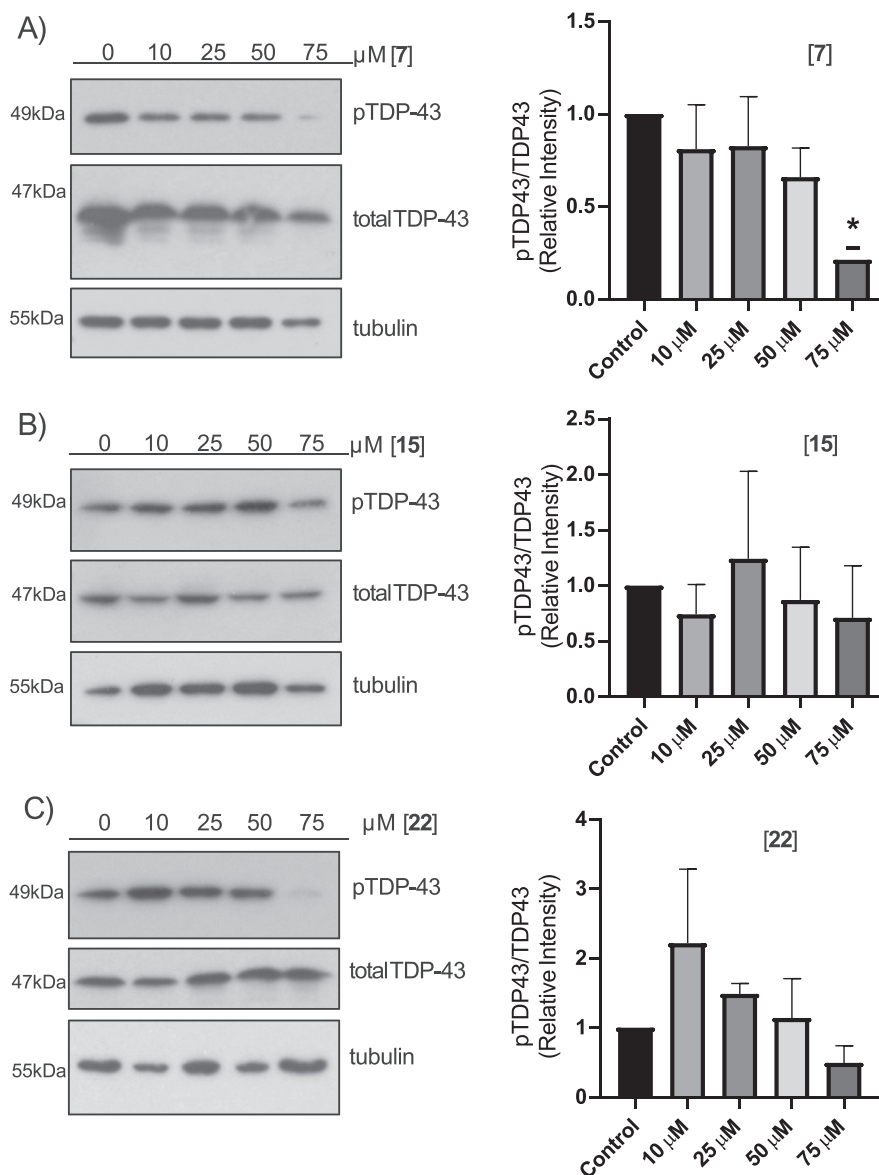


Fig. 9. Effects of CDC7 inhibitors on TDP-43 phosphorylation in *C. elegans*. Stage-matched populations of transgenic *C. elegans* expressing human TDP-43 (M337V) were grown in the presence of control (DMSO) or the indicated concentration of inhibitor for 6 days. (A) *C. elegans* treated with compound **7** had significantly decreased levels of TDP-43 phosphorylation at 75 μM. Data represent the mean ± SEM of 4 different experiments. p-values, one-way ANOVA with Dunnett's multiple comparisons test versus Control: 10 μM, 0.867; 25 μM, 0.896; 50 μM, 0.490; 75 μM, 0.024. (B) *C. elegans* treated with compound **15** had no significant changes to the levels of TDP-43 phosphorylation. p-values, one-way ANOVA with Dunnett's multiple comparisons test versus Control: 10 μM, 0.985; 25 μM, 0.988; 50 μM, 0.999; 75 μM, 0.977. (C) compound **22** had no significant changes to the levels of TDP-43 phosphorylation. p-values, one-way ANOVA with Dunnett's multiple comparisons test versus Control: 10 μM, 0.387; 25 μM, 0.922; 50 μM, 0.999; 75 μM, 0.913.

inhibitors. These compounds have shown an ATP competitive binding mode but with a wide selectivity over more than 40 structurally related kinases. Furthermore, these CDC7 inhibitors are predicted to cross the BBB using a PAMPA methodology and are able to reduce TDP-43 phosphorylation both in human cell lines and *in vivo* *C. elegans* model with overexpression of hTDP-43. Finally, all these data have been confirmed in a TDP-43 (A315T) transgenic mice model, where chronic administration of one of mercaptopurine-based CDC7 inhibitors here described, compound **22**, produced a decrease in the severity of the clinical symptoms of the disease and an *in vivo* reduction of TDP-43 phosphorylation in the spinal cord of the animals.

Altogether, purine-based CDC7 inhibitors here reported are valuable pharmacological tools for the study of the role of CDC7 in

neurological conditions and promising candidates to be developed as innovative drugs for the pharmacotherapy of ALS and others TDP-43-pathies.

3.1. Experimental part

3.1.1. Chemistry

All reagents and solvents were used as commercially available. Melting points were determined with a Büchi Melting Point M – 560 apparatus. Flash column chromatography was performed at medium pressure using silica gel (Merck, grade 60, particle size 0.040–0.063 mm, 230–400 mesh ASTM) with the indicated solvent as eluent. For TLC analyses, silica plates (Merck, silica gel 60 F254) were used. Spots were visualized under UV light (254 nm). ¹H

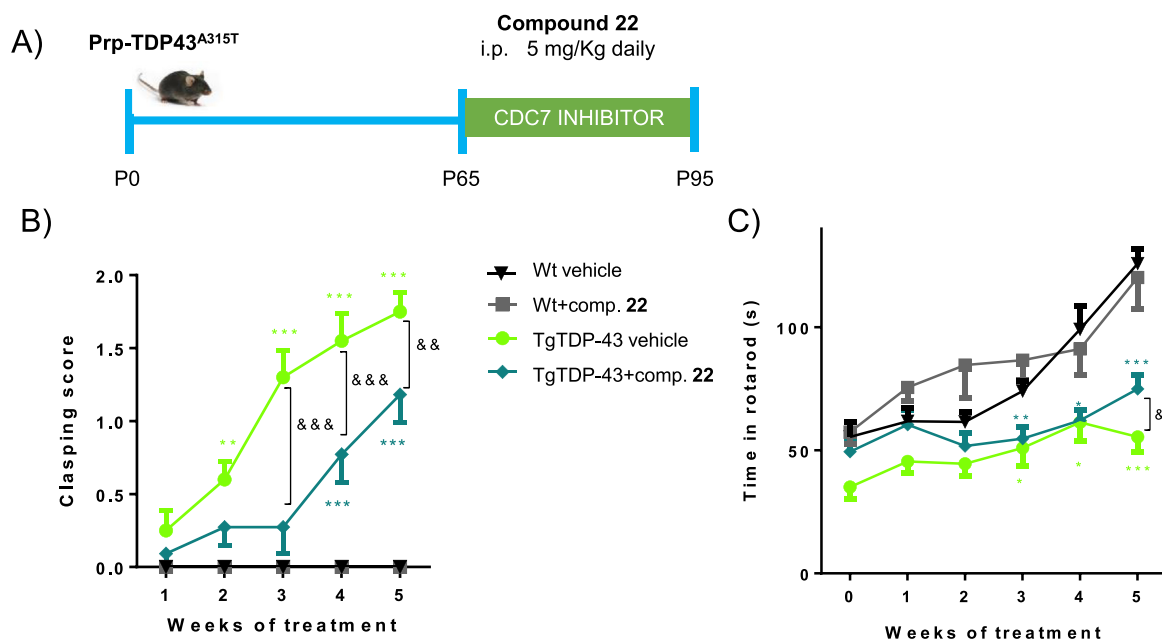


Fig. 10. Experimental design (A) and behavioral studies (B, C). (B) Hindlimb claspings and (C) rotarod test results of wild-type and transgenic TDP-43 (A315T) mice treated with compound 22 or vehicle. Values are expressed as means \pm SEM; $N \geq 6$ animals in each group. Two-way ANOVA test was used for statistical analysis followed by the Tukey's multiple comparisons test ($*p < 0.05$, $**p < 0.01$, $***p < 0.001$ vs. WT-Veh group; $&p < 0.05$, $&&p < 0.01$, $&&&p < 0.001$ vs. TDP-43-Veh group)

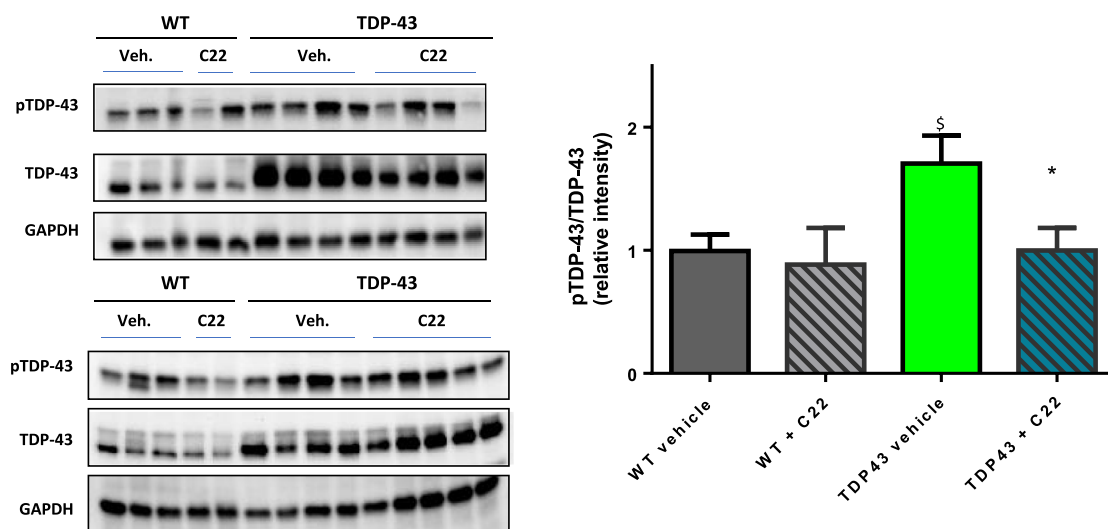


Fig. 11. Phosphorylated TDP-43 levels in the spinal cord of wild-type and transgenic TDP-43 (A315T) mice treated with compound 22 or vehicle. Representative immunoblots are shown. Data represent the mean \pm SEM of 8 observations per group. Data were assessed by one-way ANOVA followed by the Bonferroni test ($\$p < 0.05$ vs. WT-Veh group, $*p < 0.05$ vs. TDP43-Veh group).

NMR spectra were obtained on a Bruker AVIII 300 MHz BACS-60 spectrometer working at 300 MHz or on a Bruker AV 500 MHz spectrometer working at 500 MHz. ^{13}C NMR experiments were carried out on a Bruker AVIII 300 MHz BACS-60 spectrometer working at 75 MHz or on a Bruker AV 500 MHz spectrometer working at 125 MHz. Chemical shifts are reported in ppm relative to TMS as internal standard and J values are reported in Hertz. Mass spectra were obtained by electrospray ionization (ESI) with a Thermo Mod. FinniganTM LXQ TM spectrometer with on line HPLC Surveyor. HPLC analyses were performed on the same equipment, with a Photo Diode Array detector (Surveyor PDA Plus), using a

Sunfire column C18, 3.5 μM (50 mm \times 4.6 mm) and acetonitrile and Milli-Q water as a mobile phase. Both solvents contain 1% of formic acid. The standard gradient consisted of a 15 min run from 10% to 90% of acetonitrile at a flow rate of 1 mL/min. Microwave assisted reactions were performed on a Biotage Initiator + instrument from Biotage. Purity of the tested compounds was evaluated by elemental analyses performed at the Centre of Elemental Micro-analysis, Complutense University of Madrid (Spain). The results obtained were within $\pm 0.4\%$ of the theoretical values.

Synthesis and structural elucidation of compounds **1–7**, **7b**, **9–10**, **12**, **14**, **20**, **30–32**, **34** and **36** are collected in the [supporting](#)

information.

3.1.2. General procedure B

A solution of 6-mercaptopurine monohydrate (1 eq.) and K_2CO_3 (1 eq.) in DMF (25 mL) is stirred for 1 h at room temperature. Then, the appropriate benzyl derivative (1 eq.) is added and the mixture is stirred for 2–16 h at room temperature. The solvent is evaporated under low pressure and EtOAc (100 mL) is added. The organic phase is washed with distilled water (3×100 mL), adding NaCl and dried over Mg_2SO_4 anhydrous, filtered and concentrated to dryness. Finally, the crude is purified by column chromatography using $CH_2Cl_2/MeOH$ (10:1) as eluent.

3.1.3. 6-[(4-Iodobenzyl)thio]-9H-purine (**8**)

The compound was prepared from 6-mercaptopurine monohydrate (0.30 g, 1.8 mmol) and 4-iodobenzyl bromide (0.52 g, 1.8 mmol) according to general procedure B to yield **8** (572 mg; 88%). White solid. Mp 216–218 °C. 1H NMR (DMSO- d_6): δ 4.60 (s, 2H, CH_2), 7.27 (d, $J = 8.0$ Hz, 2H, Ph), 7.66 (d, $J = 8.0$ Hz, 2H, Ph), 8.45 (s, 1H), 8.72 (s, 1H), 13.54 (s, 1H, NH). ^{13}C NMR (DMSO- d_6): δ 31.0, 93.0, 129.0, 131.3, 137.2, 138.0, 143.5, 150.3, 151.4, 157.1. Anal. ($C_{12}H_9IN_4S$) Calculated: C, 39.14; H, 2.46; N, 15.22; S, 8.71. Found: C, 38.99; H, 2.57; N, 15.02; S, 8.79.

3.1.4. 6-[(4-(Methylthio)benzyl)thio]-9H-purine (**11**)

The compound was prepared from 6-mercaptopurine monohydrate (0.30 g, 1.8 mmol) and 4-(methylthio)benzyl bromide (0.38 g, 1.8 mmol) according to general procedure B to yield **11** (158 mg; 31%). White solid. Mp 203–205 °C. 1H NMR (DMSO- d_6): δ 2.44 (s, 3H, CH_3), 4.61 (s, 2H, CH_2), 7.20 (d, $J = 8.0$ Hz, 2H, Ph), 7.40 (d, $J = 8.0$ Hz, 2H, Ph), 8.44 (s, 1H), 8.73 (s, 1H), 13.53 (s, 1H, NH). ^{13}C NMR (DMSO- d_6): δ 14.7, 31.2, 126.0, 129.6, 130.1, 134.5, 136.9, 143.0, 149.3, 151.4, 158.2. MS (ES): m/z 289 (M+1). Anal. ($C_{13}H_{12}N_4S_2$) Calculated: C, 54.14; H, 4.19; N, 19.43; S, 22.24. Found: C, 53.96; H, 4.15; N, 19.34; S, 22.19.

3.1.5. 4-[(9H-Purin-6-ylthio)methyl]-benzenemethanol (**13**)

The compound was prepared from 6-mercaptopurine monohydrate (0.30 g, 1.8 mmol) and 4-(bromomethyl)phenylmethanol (0.35 g, 1.8 mmol) according to general procedure B to yield **13** (160 mg; 33%). Beige solid. Mp 226–228 °C. 1H NMR (DMSO- d_6): δ 4.45 (s, 2H, CH_2), 4.46 (s, 2H, CH_2OH), 5.13 (s, 1H, OH), 7.25 (d, $J = 8.0$ Hz, 2H, Ph), 7.41 (d, $J = 8.0$ Hz, 2H, Ph), 8.44 (s, 1H), 8.73 (s, 1H), 13.52 (s, 1H, NH). ^{13}C NMR (DMSO- d_6): δ 34.5, 62.6, 126.6, 128.7, 129.0, 136.0, 141.5, 143.4, 150.2, 151.4, 157.5. Anal. ($C_{13}H_{12}N_4OS$) Calculated: C, 57.34; H, 4.44; N, 20.57; S, 11.77. Found: C, 57.17; H, 4.62; N, 20.14; S, 11.45.

3.1.6. 6-[(3-Chlorobenzyl)thio]-9H-purine (**15**) and 9-(3-chlorobenzyl)-6-[(3-chlorobenzyl)thio]-9H-purine (**15b**)

The compounds were prepared from 6-mercaptopurine monohydrate (0.30 g, 1.8 mmol) and 3-chlorobenzyl bromide (0.36 g, 1.8 mmol) according to general procedure B. Purification: first fraction, disubstituted derivative **15b** (33 mg; 9%). White solid. Mp 98–100 °C. 1H NMR (DMSO- d_6): δ 4.63 (s, 2H, CH_2), 5.39 (s, 2H, CH_2), 7.15 (dd, $J = 6.0, 3.0, 2.0$ Hz, 1H, Ph), 7.17–7.26 (m, 2H, Ph), 7.22–7.34 (m, 3H, Ph), 7.36 (dd, $J = 6.0, 3.0, 2.0$ Hz, 1H, Ph), 7.48 (s, 1H, Ph), 7.95 (s, 1H), 8.77 (s, 1H). ^{13}C NMR (DMSO- d_6): δ 32.2, 46.9, 125.9, 127.5, 127.6, 128.0, 129.0, 129.4, 129.9, 130.6, 131.1, 134.4, 135.2, 137.2, 139.9, 142.5, 148.8, 152.3, 160.4. MS (ES): m/z 405 (M+5), 403 (M+3), 401 (M+1). Anal. ($C_{19}H_{14}Cl_2N_4S$) Calculated: C, 56.86; H, 3.52; N, 13.96; S, 7.99. Found: C, 56.87; H, 3.53; N, 13.86; S, 7.95.

Purification: second fraction, monosubstituted derivative **15** (233 mg; 48%). White solid. Mp 167–169 °C (lit [46], 168 °C). 1H

NMR (DMSO- d_6): δ 4.66 (s, 2H, CH_2), 7.30 (dt, $J = 8.0, 2.0$ Hz, 1H, Ph), 7.40–7.25 (m, 1H, Ph), 7.44 (dt, $J = 7.0, 2.0$ Hz, 1H, Ph), 7.54 (s, 1H, Ph), 8.46 (s, 1H), 8.74 (s, 1H), 13.56 (s, 1H, NH). ^{13}C NMR (DMSO- d_6): δ 30.9, 127.1, 127.7, 128.8, 130.3, 132.9, 140.8, 143.4, 149.5, 151.4, 157.3. MS (ES): m/z 279 (M+3), 277 (M+1). Anal. ($C_{12}H_9ClN_4S$) Calculated: C, 52.08; H, 3.28; N, 20.24; S, 11.59. Found: C, 51.98; H, 3.28; N, 20.21; S, 11.68.

3.1.7. 6-[(3-Nitrobenzyl)thio]-9H-purine (**16**)

The compound was prepared from 6-mercaptopurine monohydrate (0.30 g, 1.8 mmol) and 3-nitrobenzyl bromide (0.38 g, 1.8 mmol) according to general procedure B to yield **16** (461 mg; 91%). Pale yellow solid. Mp 193–195 °C. 1H NMR (DMSO- d_6): δ 4.79 (s, 2H, CH_2), 7.60 (t, $J = 8.0$ Hz, 1H, Ph), 7.94 (dt, $J = 8.0, 1.0$ Hz, 1H, Ph), 8.09 (dd, $J = 8.0, 2.0, 1.0$ Hz, 1H, Ph), 8.36 (t, $J = 2.0$ Hz, 1H, Ph), 8.47 (s, 1H, Ph), 8.74 (s, 1H), 13.58 (s, 1H, NH). ^{13}C NMR (DMSO- d_6): δ 30.6, 122.0, 123.6, 129.9 (2C), 135.7, 140.9, 143.6, 147.7, 150.2, 151.4, 156.8. Anal. ($C_{12}H_9N_5O_2S$) Calculated: C, 50.17; H, 3.16; N, 24.38; S, 11.16. Found: C, 50.07; H, 2.76; N, 24.15; S, 11.05.

3.1.8. 6-[(3-Iodobenzyl)thio]-9H-purine (**17**)

The compound was prepared from 6-mercaptopurine monohydrate (0.30 g, 1.8 mmol) and 3-iodobenzyl bromide (0.52 g, 1.8 mmol) according to general procedure B to yield **17** (380 mg; 58%). Pale yellow solid. Mp 185–187 °C. 1H NMR (DMSO- d_6): δ 4.61 (s, 2H, CH_2), 7.11 (t, $J = 8.0$ Hz, 1H, Ph), 7.48 (dt, $J = 8.0, 2.0$ Hz, 1H, Ph), 7.60 (dt, $J = 8.0, 2.0$ Hz, 1H, Ph), 7.85 (t, $J = 2.0$ Hz, 1H, Ph), 8.46 (s, 1H, Ph), 8.74 (s, 1H), 13.56 (s, 1H, NH). ^{13}C NMR (DMSO- d_6): δ 30.7, 94.7, 128.4, 129.8, 130.6, 135.8, 137.5, 140.9, 143.4, 149.8, 151.4, 157.3. Anal. ($C_{12}H_9IN_4S$) Calculated: C, 39.14; H, 2.46; N, 15.22; S, 8.71. Found: C, 39.26; H, 2.53; N, 15.05; S, 8.58.

3.1.9. 6-[(3-(Trifluoromethyl)benzyl)thio]-9H-purine (**18**)

The compound was prepared from 6-mercaptopurine monohydrate (0.30 g, 1.8 mmol) and 3-(trifluoromethyl)benzyl bromide (0.42 g, 1.8 mmol) according to general procedure B to yield **18** (283 mg; 52%). White solid. Mp 180–182 °C. 1H NMR (DMSO- d_6): δ 4.74 (s, 2H, CH_2), 7.54 (t, $J = 8.0$ Hz, 1H, Ph), 7.61 (d, $J = 8.0$ Hz, 1H, Ph), 7.79 (d, $J = 8.0$ Hz, 1H, Ph), 7.86 (s, 1H, Ph), 8.46 (s, 1H), 8.74 (s, 1H), 13.57 (s, 1H, NH). ^{13}C NMR (DMSO- d_6): δ 30.9, 123.8 (q, $J = 4.0$ Hz), 118.6–129.8 (m), 125.5 (q, $J = 4.0$ Hz), 129.1 (q, $J = 32.0$ Hz), 129.5, 133.1, 139.9, 143.5, 150.3, 151.4, 157.2. MS (ES): m/z 311 (M+1). Anal. ($C_{13}H_9F_3N_4S$) Calculated: C, 50.32; H, 2.92; N, 18.06; S, 10.33. Found: C, 50.49; H, 3.03; N, 18.03; S, 10.32.

3.1.10. 3-[(9H-Purin-6-ylthio)methyl]-benzonitrile (**19**)

The compound was prepared from 6-mercaptopurine monohydrate (0.30 g, 1.8 mmol) and 3-cyanobenzyl bromide (0.35 g, 1.8 mmol) according to general procedure B to yield **19** (439 mg; 93%). White solid. Mp 189–191 °C. 1H NMR (DMSO- d_6): δ 4.70 (s, 2H, CH_2), 7.52 (t, $J = 8.0$ Hz, 1H, Ph), 7.71 (dt, $J = 8.0, 2.0$ Hz, 1H, Ph), 7.82 (dt, $J = 8.0, 2.0$ Hz, 1H, Ph), 7.93 (t, $J = 2.0$ Hz, 1H, Ph), 8.46 (s, 1H), 8.74 (s, 1H), 13.57 (s, 1H, NH). ^{13}C NMR (DMSO- d_6): δ 30.7, 111.3, 118.6, 129.7 (2C), 130.9, 132.4, 133.9, 140.1, 143.5, 150.2, 151.4, 156.9. MS (ES): m/z 268 (M+1). Anal. ($C_{13}H_9N_5S$) Calculated: C, 58.41; H, 3.39; N, 26.20; S, 12.00. Found: C, 58.46; H, 3.47; N, 26.03; S, 11.84.

3.1.11. 6-[3-(Fluorobenzyl)thio]-9H-purine (**21**)

The compound was prepared from 6-mercaptopurine monohydrate (0.30 g, 1.8 mmol) and 3-fluorobenzyl bromide (0.33 g, 1.8 mmol) according to general procedure B to yield **21** (286 mg; 62%). White solid. Mp 147–148 °C. 1H NMR (DMSO- d_6): δ 4.67 (s, 2H, CH_2), 7.07 (tt, $J = 8.0, 2.0$ Hz, 1H, Ph), 7.32 (s, 1H, Ph), 7.24–7.43 (m, 2H, Ph), 8.46 (s, 1H), 8.74 (s, 1H), 13.56 (s, 1H, NH). ^{13}C NMR (DMSO- d_6): δ 30.9, 114.0 (d, $J = 21.0$ Hz), 115.7 (d, $J = 22.0$ Hz), 125.1

(d, $J = 3.0$ Hz), 130.1, 130.4 (d, $J = 8.0$ Hz), 141.1 (d, $J = 8.0$ Hz), 143.1, 149.4, 151.4, 157.8, 162.0 (d, $J = 244.0$ Hz). HPLC: purity 99%, r. t. 9.56 min. MS (ES): m/z 261 (M+1). Anal. (C₁₂H₉FN₄S) Calculated: C, 55.37; H, 3.49; N, 21.53; S, 12.32. Found: 54.98; H, 3.72; N, 21.16; S, 11.92.

3.1.12. 6-[(2-Bromobenzyl)thio]-9H-purine (**22**)

The compound was prepared from 6-mercaptapurine monohydrate (0.30 g, 1.8 mmol) and 2-bromobenzyl bromide (0.44 g, 1.8 mmol) according to general procedure B to yield **22** (462 mg; 82%). White solid. Mp 209–211 °C. ¹H NMR (DMSO-*d*₆): δ 4.74 (s, 2H, CH₂), 7.22 (td, $J = 8.0, 2.0$ Hz, 1H, Ph), 7.33 (td, $J = 8.0, 2.0$ Hz, 1H, Ph), 7.66 (dt, $J = 8.0, 2.0$ Hz, 2H, Ph), 8.45 (s, 1H), 8.76 (s, 1H), 13.58 (s, 1H, NH). ¹³C NMR (DMSO-*d*₆): δ 32.4, 124.2, 128.0, 129.6, 130.1, 131.5, 132.8, 136.8, 143.2, 149.4, 151.5, 157.7. Anal. (C₁₂H₉BrN₄S) Calculated: C, 44.87; H, 2.82; N, 17.44; S, 9.98. Found: C, 44.96; H, 2.83; N, 17.43; S, 9.97.

3.1.13. 6-[(2-Chlorobenzyl)thio]-9H-purine (**23**) and 9-(2-chlorobenzyl)-6-[(2-chlorobenzyl)thio]-9H-purine (**23b**)

The compounds were prepared from 6-mercaptapurine monohydrate (0.30 g, 1.8 mmol) and 2-chlorobenzyl bromide (0.36 g, 1.8 mmol) according to general procedure B. Purification: first fraction, disubstituted derivative **23b** (119 mg; 34%). White solid. Mp 135–137 °C. ¹H NMR (DMSO-*d*₆): δ 4.75 (s, 2H, CH₂), 5.58 (s, 2H, CH₂), 7.08 (dd, $J = 8.0, 2.0$ Hz, 1H, Ph), 7.27 (dd, $J = 8.0, 2.0$ Hz, 1H, Ph), 7.23–7.36 (m, 2H, Ph), 7.37 (dd, $J = 8.0, 2.0$ Hz, 1H, Ph), 7.46–7.50 (m, 1H, Ph), 7.51 (dd, $J = 6.0, 2.0$ Hz, 1H, Ph), 7.60–7.72 (m, 1H, Ph), 8.55 (s, 1H), 8.77 (s, 1H). ¹³C NMR (DMSO-*d*₆): δ 29.7, 44.7, 127.4, 127.6, 129.3, 129.5, 129.5, 129.6, 129.8, 130.3, 131.4, 132.1, 133.3, 133.4, 135.0, 145.1, 148.7, 151.6, 158.4. MS (ES): m/z 405 (M+5), 403 (M+3), 401 (M+1). Anal. (C₁₉H₁₄Cl₂N₄S) Calculated: C, 56.86; H, 3.52; N, 13.96; S, 7.99. Found: C, 57.08; H, 3.56; N, 14.01; S, 7.94.

Purification: second fraction, monosubstituted derivative **23** (236 mg; 48%). White solid. Mp 200–202 °C. ¹H NMR (DMSO-*d*₆): δ 4.75 (s, 2H, CH₂), 7.26–7.35 (m, 2H, Ph), 7.49 (dd, $J = 7.0, 3.0$ Hz, 1H, Ph), 7.66 (dd, $J = 6.0, 3.0$ Hz, 1H, Ph), 8.46 (s, 1H), 8.76 (s, 1H), 13.56 (s, 1H, NH). ¹³C NMR (DMSO-*d*₆): δ 29.7, 127.4, 129.3, 129.5, 130.5, 131.4, 133.4, 135.1, 143.3, 149.4, 151.4, 157.6. MS (ES): m/z 279 (M+3), 277 (M+1). Elem. (C₁₂H₉ClN₄S) Calculated: C, 52.08; H, 3.28; N, 20.24; S, 11.59. Found: C, 52.12; H, 3.33; N, 20.08; S, 11.38.

3.1.14. 6-[(2-Iodobenzyl)thio]-9H-purine (**24**) and 9-(2-iodobenzyl)-6-[(2-iodobenzyl)thio]-9H-purine (**24b**)

The compounds were prepared from 6-mercaptapurine monohydrate (0.30 g, 1.8 mmol) and 2-iodobenzyl bromide (0.52 g, 1.8 mmol) according to general procedure B. Purification: first fraction, disubstituted derivative **24b** (22 mg; 4%). Beige solid. Mp 150–152 °C. ¹H NMR (DMSO-*d*₆): δ 4.74 (s, 2H, CH₂), 5.46 (s, 2H, CH₂), 6.82 (dd, $J = 8.0, 2.0$ Hz, 1H, Ph), 6.98–7.15 (m, 2H, Ph), 7.32 (td, $J = 8.0, 2.0$ Hz, 1H, Ph), 7.36 (td, $J = 8.0, 2.0$ Hz, 1H, Ph), 7.66 (dd, $J = 8.0, 2.0$ Hz, 1H, Ph), 7.90 (dd, $J = 8.0, 2.0$ Hz, 1H, Ph), 7.94 (dd, $J = 8.0, 2.0$ Hz, 1H, Ph), 8.50 (s, 1H), 8.78 (s, 1H). ¹³C NMR (DMSO-*d*₆): δ 37.2, 51.6, 98.2, 101.4, 128.4, 128.6, 128.8, 129.5, 129.9, 130.3, 130.8, 137.8, 139.3, 139.4, 139.8, 145.1, 148.7, 151.7, 158.5. HPLC: purity 99%, r. t. 10.60 min. MS (ES): m/z 585 (M+1). Anal. (C₁₉H₁₄I₂N₄S) Calculated: C, 39.06; H, 2.42; N, 9.59; S, 5.49. Found: C, 39.46; H, 2.75; N, 9.54; S, 5.30.

Purification: second fraction, monosubstituted derivative **24** (541 mg; 83%). White solid. Mp 215–217 °C. ¹H NMR (DMSO-*d*₆): δ 4.72 (s, 2H, CH₂), 7.03 (td, $J = 8.0, 2.0$ Hz, 1H, Ph), 7.35 (td, $J = 8.0, 1.0$ Hz, 1H, Ph), 7.64 (dd, $J = 8.0, 2.0$ Hz, 1H, Ph), 7.89 (dd, $J = 8.0, 1.0$ Hz, 1H, Ph), 8.44 (s, 1H), 8.75 (s, 1H), 13.55 (s, 1H, NH). ¹³C NMR (DMSO-*d*₆): δ 37.1, 101.3, 128.6, 129.4, 130.0, 130.6, 139.3, 139.9,

143.1, 149.4, 151.4, 157.7. Anal. (C₁₂H₉ClN₄S) Calculated: C, 39.15; H, 2.46; N, 15.22; S, 8.71. Found: C, 38.95; H, 2.55; N, 15.43; S, 8.53.

3.1.15. 6-[(2-(Trifluoromethyl)benzyl)thio]-9H-purine (**25**) and 9-[2-(trifluoromethyl)benzyl]-6-[(2-(trifluoromethyl)benzyl)thio]-9H-purine (**25b**)

The compounds were prepared from 6-mercaptapurine monohydrate (0.30 g, 1.8 mmol) and 2-(trifluoromethyl)benzyl bromide (0.42 g, 1.8 mmol) according to general procedure B. Purification: first fraction, disubstituted derivative **25b** (410 mg; 99%). White solid. Mp 106–108 °C. ¹H NMR (DMSO-*d*₆): δ 4.85 (s, 2H, CH₂), 5.71 (s, 2H, CH₂), 6.93 (d, $J = 7.0$ Hz, 1H, Ph), 7.46–7.63 (m, 3H, Ph), 7.64 (t, $J = 8.0$ Hz, 1H, Ph), 7.72–7.87 (m, 3H, Ph), 8.57 (s, 1H), 8.78 (s, 1H). ¹³C NMR (DMSO-*d*₆): δ 28.0–28.5 (m), 43.5 (q, $J = 2.0$ Hz), 118.7–130.0 (m), 118.8–130.0 (m), 125.3–126.8 (m), 125.9–126.5 (m), 127.2 (q, $J = 30.0$ Hz), 128.2, 128.4, 128.4, 130.3, 131.9, 133.0, 133.2, 133.8–134.5 (m), 135.5–135.9 (m), 145.4, 148.8, 151.7, 158.2. MS (ES): m/z 469 (M+1). Anal. (C₂₁H₁₄F₆N₄S) Calculated: C, 53.85; H, 3.01; N, 11.96; S, 6.85. Found: C, 53.87; H, 2.98; N, 11.94; S, 6.85.

Purification: second fraction, monosubstituted derivative **25** (499 mg; 91%). White solid. Mp 197–199 °C. ¹H NMR (DMSO-*d*₆): δ 4.83 (s, 2H, CH₂), 7.50 (t, $J = 8.0$ Hz, 1H, Ph), 7.63 (td, $J = 8.0, 2.0$ Hz, 1H, Ph), 7.77 (t, $J = 8.0$ Hz, 2H, Ph), 8.47 (s, 1H), 8.77 (s, 1H), 13.59 (s, 1H, NH). ¹³C NMR (DMSO-*d*₆): δ 28.2, 124.4 (q, $J = 274.0$ Hz), 126.1 (q, $J = 6.0$ Hz), 127.2 (q, $J = 30.0$ Hz), 128.1, 129.8, 131.9, 133.0, 133.2–138.6 (m), 143.6, 150.5, 151.4, 156.7. Anal. (C₁₃H₉F₃N₄S) Calculated: C, 50.32; H, 2.92; N, 18.06; S, 10.33. Found: C, 50.35; H, 2.90; N, 18.05; S, 10.40.

3.1.16. General procedure C

A solution of 6-mercaptapurine monohydrate (1 eq.) and K₂CO₃ (1 eq.) in DMF is stirred for 1 h at room temperature. Then, the suitable phenethyl derivative (1 eq.) is added and the mixture is stirred for 2–5 h at room temperature. The solvent is evaporated under low pressure and EtOAc is added. The organic phase is washed with distilled water, adding NaCl and dried over Mg₂SO₄ anhydrous, filtered and concentrated to dryness. Finally, the crude is purified by column chromatography using CH₂Cl₂/MeOH (10:1) as eluent.

3.1.17. 6-[(4-Chlorophenethyl)thio]-9H-purine (**26**) and 9-(4-chlorophenethyl)-6-[(4-chlorophenethyl)thio]-9H-purine (**26b**)

The compounds were prepared from 6-mercaptapurine monohydrate (0.30 g, 1.8 mmol) and 4-chlorophenethyl bromide (0.39 g, 1.8 mmol) according to general procedure C. Purification: first fraction, disubstituted derivative **26b** (96 mg; 25%). Beige solid. Mp 93–95 °C. ¹H NMR (DMSO-*d*₆): δ 3.01 (dd, $J = 8.0, 7.0$ Hz, 2H, CH₂), 3.18 (t, $J = 7.0$ Hz, 2H, CH₂), 3.58 (dd, $J = 8.0, 7.0$ Hz, 2H, CH₂), 4.49 (t, $J = 7.0$ Hz, 2H, CH₂), 7.15 (d, $J = 8.0$ Hz, 2H, Ph), 7.29 (d, $J = 8.0$ Hz, 2H, Ph), 7.30–7.41 (m, 4H, Ph), 8.29 (s, 1H), 8.73 (s, 1H). ¹³C NMR (DMSO-*d*₆): δ 29.0, 34.2, 34.4, 44.3, 128.3, 128.4, 130.5, 130.5, 130.6, 131.0, 131.2, 136.8, 139.1, 144.5, 148.4, 151.4, 159.0. Anal. (C₂₁H₁₈Cl₂N₄S) Calculated: C, 58.75; H, 4.23; N, 13.05; S, 7.47. Found: C, 58.89; H, 4.43; N, 12.96; S, 7.35.

Purification: second fraction, monosubstituted derivative **26** (315 mg; 62%). White solid. Mp 190–192 °C. ¹H NMR (DMSO-*d*₆): δ 3.02 (t, $J = 8.0$ Hz, 2H, CH₂), 3.59 (t, $J = 8.0$ Hz, 2H, CH₂), 7.18–7.55 (m, 4H, Ph), 8.44 (s, 1H), 8.71 (s, 1H), 13.51 (s, 1H, NH). ¹³C NMR (DMSO-*d*₆): δ 29.0, 34.4, 128.3, 130.0, 130.5, 131.0, 139.1, 143.3, 149.6, 151.5, 158.2. Anal. (C₁₃H₁₁ClN₄S) Calculated: C, 53.70; H, 3.81; N, 19.27; S, 11.03. Found: C, 53.37; H, 3.79; N, 19.03; S, 10.85.

3.1.18. 6-[(4-Fluorophenethyl)thio]-9H-purine (**27**) and 9-(4-fluorophenethyl)-6-[(4-fluorophenethyl)thio]-9H-purine (**27b**)

The compounds were prepared from 6-mercaptapurine

monohydrate (0.30 g, 1.8 mmol) and 4-fluorophenethyl bromide (0.36 g, 1.8 mmol) according to general procedure C. Purification: first fraction, disubstituted derivative **27b** (47 mg; 17%). White solid. Mp 112–113 °C. ¹H NMR (DMSO-*d*₆): δ 3.00 (t, *J* = 8.0 Hz, 2H, CH₂), 3.17 (t, *J* = 7.0 Hz, 2H, CH₂), 3.58 (dd, *J* = 8.0, 7.0 Hz, 2H, CH₂), 4.48 (t, *J* = 7.0 Hz, 2H, CH₂), 7.01–7.10 (m, 2H, Ph), 7.11–7.20 (m, 4H, Ph), 7.27–7.41 (m, 2H, Ph), 8.28 (s, 1H), 8.73 (s, 1H). ¹³C NMR (DMSO-*d*₆): δ 29.3, 34.1, 34.3, 44.5, 115.0 (d, *J* = 9.0 Hz), 115.3 (d, *J* = 9.0 Hz), 130.4 (d, *J* = 8.0 Hz), 130.5 (d, *J* = 8.0 Hz), 130.6, 133.9 (d, *J* = 3.0 Hz), 136.2 (d, *J* = 3.0 Hz), 144.5, 148.4, 151.4, 159.0, 160.9 (d, *J* = 242.0 Hz), 161.0 (d, *J* = 242.0 Hz). HPLC: purity 99%, r. t. 9.53 min. MS (ES): *m/z* 397 (M+1). Anal. (C₂₁H₁₈F₂N₄S) Calculated: C, 63.62; H, 4.58; N, 14.13; S, 8.09. Found: C, 62.83; H, 4.48; N, 13.81; S, 7.94.

Purification: second fraction, monosubstituted derivative **27** (285 mg; 59%). White solid. Mp 184–186 °C. ¹H NMR (DMSO-*d*₆): δ 3.02 (t, *J* = 8.0 Hz, 2H, CH₂), 3.59 (t, *J* = 8.0 Hz, 2H, CH₂), 6.94–7.22 (m, 2H, Ph), 7.26–7.45 (m, 2H, Ph), 8.42 (s, 1H), 8.70 (s, 1H), 13.51 (s, 1H, NH). ¹³C NMR (DMSO-*d*₆): δ 29.2, 34.3, 115.0 (d, *J* = 21.0 Hz), 130.4, 130.4 (d, *J* = 8.0 Hz), 136.3 (d, *J* = 3.0 Hz), 142.9, 149.2, 151.5, 158.6, 160.9 (d, *J* = 242.0 Hz). HPLC: purity 99%, r. t. 6.99 min. MS (ES): *m/z* 275 (M+1). Anal. (C₁₃H₁₁FN₄S) Calculated: C, 56.92; H, 4.04; N, 20.42; S, 11.69. Found: C, 56.58; H, 4.01; N, 20.04; S, 11.43.

3.1.19. 6-[(3-Chlorophenethyl)thio]-9H-purine (28) and 9-(3-chlorophenethyl)-6-[(3-chlorophenethyl)thio]-9H-purine (28b)

The compounds were prepared from 6-mercaptapurine monohydrate (0.30 g, 1.8 mmol) and 3-chlorophenethyl bromide (0.39 g, 1.8 mmol) according to general procedure C. Purification: first fraction, disubstituted derivative **28b** (22 mg; 6%). White solid. Mp 137–139 °C. ¹H NMR (DMSO-*d*₆): δ 3.03 (t, *J* = 8.0 Hz, 2H, CH₂), 3.19 (t, *J* = 7.0 Hz, 2H, CH₂), 3.61 (dd, *J* = 8.0, 7.0 Hz, 2H, CH₂), 4.51 (t, *J* = 7.0 Hz, 2H, CH₂), 7.05–7.09 (m, 1H, Ph), 7.22–7.26 (m, 2H, Ph), 7.27 (t, *J* = 2.0 Hz, 1H, Ph), 7.28 (dt, *J* = 8.0, 2.0 Hz, 2H, Ph), 7.33 (t, *J* = 8.0 Hz, 1H, Ph), 7.39 (t, *J* = 2.0 Hz, 1H, Ph), 8.32 (s, 1H), 8.73 (s, 1H). ¹³C NMR (DMSO-*d*₆): δ 28.9, 34.5, 34.6, 44.1, 126.4, 126.6, 127.4, 127.4, 128.5, 128.6, 130.2, 130.2, 130.6, 133.0, 133.0, 140.3, 142.6, 144.5, 148.4, 151.4, 158.9. HPLC: purity 99%, r. t. 10.52 min. MS (ES): *m/z* 433 (M+5), 431 (M+3), 429 (M+1). Anal. (C₂₁H₁₈Cl₂N₄S) Calculated: C, 58.75; H, 4.23; N, 13.05; S, 7.47. Found: C, 58.51; H, 4.18; N, 12.89; S, 7.33.

Purification: second fraction, monosubstituted derivative **28** (402 mg; 78%). White solid. Mp 143–145 °C. ¹H NMR (DMSO-*d*₆): δ 3.04 (t, *J* = 8.0 Hz, 2H, CH₂), 3.62 (t, *J* = 8.0 Hz, 2H, CH₂), 7.24–7.37 (m, 3H, Ph), 7.39 (t, *J* = 2.0 Hz, 1H, Ph), 8.42 (s, 1H), 8.71 (s, 1H), 13.51 (s, 1H, NH). ¹³C NMR (DMSO-*d*₆): δ 28.8, 34.7, 126.4, 127.4, 128.5, 130.2, 130.4, 133.0, 142.6, 142.9, 149.2, 151.5, 158.5. Anal. (C₁₃H₁₁ClN₄S) Calculated: C, 53.70; H, 3.81; N, 19.27; S, 11.03. Found: C, 53.34; H, 3.80; N, 19.09; S, 11.00.

3.1.20. 6-[(2-Chlorophenethyl)thio]-9H-purine (29) and 9-(2-chlorophenethyl)-6-[(2-chlorophenethyl)thio]-9H-purine (29b)

The compounds were prepared from 6-mercaptapurine monohydrate (0.30 g, 1.8 mmol) and 2-chlorophenethyl bromide (0.39 g, 1.8 mmol) according to general procedure C. Purification: first fraction, disubstituted derivative **29b** (210 mg; 55%). White solid. Mp 140–142 °C. ¹H NMR (DMSO-*d*₆): δ 3.16 (dd, *J* = 8.0, 7.0 Hz, 2H, CH₂), 3.30 (t, *J* = 7.0 Hz, 2H, CH₂), 3.61 (dd, *J* = 8.0, 7.0 Hz, 2H, CH₂), 4.53 (t, *J* = 7.0 Hz, 2H, CH₂), 7.13–7.22 (m, 2H, Ph), 7.22–7.34 (m, 3H, Ph), 7.39 (dd, *J* = 7.0, 2.0 Hz, 1H, Ph), 7.43 (dd, *J* = 7.0, 2.0 Hz, 2H, Ph), 8.28 (s, 1H), 8.69 (s, 1H). ¹³C NMR (DMSO-*d*₆): δ 27.6, 32.6, 32.9, 42.9, 127.2, 127.3, 128.4, 128.7, 129.2, 129.3, 130.6, 131.1 (2C), 133.1, 133.2, 135.2, 137.3, 144.5, 148.5, 151.3, 158.7. Anal. (C₂₁H₁₈Cl₂N₄S) Calculated: C, 58.75; H, 4.23; N, 13.05; S, 7.47. Found: C, 58.58; H, 4.28; N, 12.79; S, 7.29.

Purification: second fraction, monosubstituted derivative **29**

(250 mg; 49%). White solid. Mp 154–156 °C. ¹H NMR (DMSO-*d*₆): δ 3.17 (dd, *J* = 8.0, 7.0 Hz, 2H, CH₂), 3.62 (dd, *J* = 8.0, 7.0 Hz, 2H, CH₂), 7.22–7.33 (m, 2H, Ph), 7.43 (dd, *J* = 7.0, 2.0 Hz, 1H, Ph), 7.44 (dd, *J* = 7.0, 2.0 Hz, 1H, Ph), 8.43 (s, 1H), 8.70 (s, 1H), 13.49 (s, 1H, NH). ¹³C NMR (DMSO-*d*₆): δ 27.6, 32.7, 127.2, 128.4, 129.2, 131.1, 133.1, 137.3, 143.3, 150.3, 151.4, 157.6. Anal. (C₁₃H₁₁ClN₄S) Calculated: C, 53.70; H, 3.81; N, 19.27; S, 11.03. Found: C, 53.60; H, 3.86; N, 19.14; S, 10.85.

3.1.21. General procedure D

A solution of an excess of the suitable benzyl alcohol derivative (5–10 eq.) in NaOH (2 eq.) is stirred at room temperature to NaOH solution. Then, 6-chloropurine (1 eq.) is added and the mixture is heated to reflux (100 °C) for 2–16 h. The solvent is evaporated under low pressure and EtOAc is added. The organic phase is washed with distilled water, adding NaCl and dried over Mg₂SO₄ anhydrous, filtered and concentrated to dryness. Finally, the crude is purified by column chromatography using CH₂Cl₂/MeOH (10:1) as eluent.

3.1.22. 6-[(3-Chlorobenzyl)oxy]-9H-purine (33)

The compound was prepared from 6-chloropurine (0.30 g, 1.9 mmol) and 3-chlorobenzyl alcohol (2.8 g, 19.0 mmol) according to general procedure D to yield **33** (154 mg; 30%). White solid. Mp 197–199 °C. ¹H NMR (DMSO-*d*₆): δ 5.62 (s, 2H, CH₂), 7.37–7.45 (m, 2H, Ph), 7.45–7.51 (m, 1H, Ph), 7.60 (s, 1H, Ph), 8.41 (s, 1H), 8.52 (s, 1H), 13.48 (s, 1H, NH). ¹³C NMR (DMSO-*d*₆): δ 66.7, 118.0, 126.7, 127.9, 128.0, 130.4, 133.1, 139.0, 143.0, 151.2, 155.3, 158.4. Anal. (C₁₂H₉ClN₄O) Calculated: C, 55.29; H, 3.48; N, 21.49. Found: C, 55.12; H, 3.51; N, 21.34.

3.1.23. 6-[(4-Bromobenzyl)oxy]-9H-purine (35)

The compound was prepared from 6-chloropurine (0.30 g, 1.9 mmol) and 4-bromobenzyl alcohol (1.8 g, 9.7 mmol) according to general procedure D to yield **35** (107 mg; 18%). Beige solid. Mp 211–213 °C. ¹H NMR (DMSO-*d*₆): δ 5.59 (s, 2H, CH₂), 7.48 (d, *J* = 8.0 Hz, 2H, Ph), 7.61 (d, *J* = 8.0 Hz, 2H, Ph), 8.40 (s, 1H), 8.51 (s, 1H), 13.48 (s, 1H, NH). ¹³C NMR (DMSO-*d*₆): δ 66.8, 118.1, 121.3, 130.4, 131.4, 135.9, 143.0, 151.2, 155.3, 158.5. Anal. (C₁₂H₉BrN₄O) Calculated: C, 47.24; H, 2.97; N, 18.36. Found: C, 47.06; H, 2.98; N, 18.31.

3.1.24. General procedure E

Under argon atmosphere, at 0 °C, an excess of the suitable benzyl mercaptan derivative (4 eq.) and NaH (2 eq.) are added over a solution of the suitable heterocyclic derivative (1 eq.) in DMF. Then, the mixture is stirred for one night at room temperature and neutralized with MeOH. The solvent is evaporated under low pressure and EtOAc is added. The organic phase is washed with distilled water, dried over Mg₂SO₄ anhydrous, filtered and concentrated to dryness. Finally, the crude is purified by column chromatography using Hexane/EtOAc (10:1) as eluent.

3.1.25. 4-[(3-Bromobenzyl)thio]thieno[2,3-*d*]pyrimidine (37)

The compound was prepared from 4-chlorothieno[2,3-*d*]pyrimidine (0.15 g, 0.9 mmol) and 3-bromobenzyl mercaptan (0.71 g, 3.5 mmol) according to general procedure E to yield **37** (98 mg; 33%). White solid. Mp 82–83 °C. ¹H NMR (CDCl₃): δ 4.52 (s, 2H, CH₂), 7.10 (t, *J* = 7.0 Hz, 1H, Ph), 7.20 (d, *J* = 8.0 Hz, 1H), 7.30 (d, *J* = 7.0 Hz, 1H, Ph), 7.33 (d, *J* = 7.0 Hz, 1H, Ph), 7.40 (d, *J* = 6.0 Hz, 1H), 7.54 (s, 1H, Ph), 8.78 (s, 1H). ¹³C NMR (CDCl₃): δ 31.5, 117.8, 121.5, 125.4, 126.5, 126.7, 129.0, 129.5, 131.1, 138.6, 151.3, 162.2, 164.8. Anal. (C₁₃H₉BrN₂S₂) Calculated: C, 46.30; H, 2.69; N, 8.31; S, 19.01. Found: C, 46.65; H, 2.88; N, 8.14; S, 18.62.

3.1.26. 4-(Benzylthio)-7H-pyrrolo[2,3-d]pyrimidine (**38**)

The compound was prepared from 4-chloro-7H-pyrrolo[2,3-d]pyrimidine (0.15 g, 1.0 mmol) and benzyl mercaptan (0.49 g, 3.9 mmol) according to general procedure E to yield **38** (164 mg; 70%). White solid. Mp 167–168 °C. ¹H NMR (DMSO-*d*₆): δ 4.68 (s, 2H, CH₂), 6.52 (dd, *J* = 4.0, 2.0 Hz, 1H), 7.26–7.50 (m, 6H), 8.69 (s, 1H), 12.25 (s, 1H, NH). ¹³C NMR (DMSO-*d*₆): δ 31.6, 98.2, 114.7, 125.8, 127.0, 128.4, 128.9, 138.0, 149.0, 150.2, 158.7. Anal. (C₁₃H₁₁N₃S) Calculated: C, 64.71; H, 4.59; N, 17.41; S, 13.29. Found: C, 64.59; H, 4.64; N, 17.28; S, 13.22.

3.1.27. 4-[(3-Bromobenzyl)thio]-7H-pyrrolo[2,3-d]pyrimidine (**39**)

The compound was prepared from 4-chloro-7H-pyrrolo[2,3-d]pyrimidine (0.15 g, 1.0 mmol) and 3-bromobenzyl mercaptan (0.79 g, 3.9 mmol) according to general procedure E to yield **39** (166 mg; 53%). White solid. Mp 188–189 °C. ¹H NMR (DMSO-*d*₆): δ 4.68 (s, 2H, CH₂), 6.52 (dd, *J* = 4.0, 2.0 Hz, 1H), 7.32 (t, *J* = 8.0 Hz, 1H, Ph), 7.46–7.56 (m, 3H), 7.73 (s, 1H, Ph), 8.69 (s, 1H), 12.26 (s, 1H, NH). ¹³C NMR (DMSO-*d*₆): δ 30.8, 98.2, 114.8, 121.4, 125.9, 128.0, 129.9, 130.5, 131.5, 141.2, 149.0, 150.2, 158.2. Anal. (C₁₃H₁₀BrN₃S) Calculated: C, 48.76; H, 3.15; N, 13.12; S, 10.01. Found: C, 48.69; H, 3.20; N, 13.11; S, 10.12.

3.1.28. Molecular docking

The protein-ligand docking was performed using Glide [47,48] and related Schrödinger packages. The reliability of Glide was assessed by docking the ADP and PHA-767491, a known CDC7 inhibitor, taking advantage of the X-ray crystallographic structures of their complexes with the enzyme (PDB entries: 4F99, 4F9A, and 4F9B) [33]. The docking of the novel CDC7 inhibitors was performed using the X-ray structure of the protein in complex with PHA-767491 (PDB entry: 4F9B). Before docking calculations, the protein was prepared using Maestro Protein Preparation Wizard [49,50], removing ligands, metals and water molecules, adding hydrogens, ionizing residues at pH 7.5 and filling in missing side chains using Prime. Minimization of the protein structure was done with OPLS3 force field. CDC7 inhibitors were also prepared using OPLS force field to minimize energy. The docking volume was defined as the space within 10 Å of the ligand PHA-767491 found in the CDC7 crystal. The docking was performed with Glide standard precision (SP) function [51], and the top-10 poses per docked ligand were selected for further analysis. The output docking modes were analyzed by visual inspection in conjunction with the docking scores.

3.1.29. Rescore of docking poses using MM-GBSA

Molecular mechanics generalized Born surface area (MM-GBSA) calculations of the different poses per ligand obtained with the molecular docking were performed using Prime. This computational method combines molecular mechanics energy and implicit solvation models that enables to rescore the docking results and correlate the experimental activities (IC₅₀) with the predicted binding energies (ΔG_{bind}) [51]. The binding free energies between the ligands and the receptor were calculated as the following:

$$\Delta G_{\text{bind}} = \Delta H - T\Delta S \approx \Delta E_{\text{MM}} + \Delta G_{\text{sol}} - T\Delta S$$

where ΔE_{MM} includes internal (bond, angle, and dihedral energies), electrostatic and van der Waals energies changes. ΔG_{sol} is the solvation free energy expressed as the sum of electrostatic and non-electrostatic solvation energies (ΔG_{PB/GB} + ΔG_{SA}). Finally, ΔS is the change of conformational entropy at a specific temperature and corrections for these changes were not applied because here we used the predicted ΔG_{bind} to rescore docking solutions.

3.2. Biology

3.2.1. In vitro inhibition of CDC7 human recombinant kinase

The inhibition experiments were performed by Life Technologies (Thermo Fisher Scientific) using the LanthaScreen Eu Kinase Binding Assay [52]. The test compounds were screened in 1% DMSO (final) in the well. For 10 points titrations, 3-fold serial dilutions were conducted from the starting concentration (10 mM). The Kinase (CDC7/DBF4)/Antibody (Eu-*anti*-GST) mixture was diluted to a 2X working concentration (0.5 nM/2 nM) in the appropriate Kinase Buffer (50 mM HEPES pH 7.5, 0.01% BRIJ-35, 10 mM MgCl₂, 1 mM EGTA). The 4X AlexaFluor labeled Tracer (Tracer 236, 1 nM) was prepared in Kinase Buffer. The 100X test compound in 100% DMSO (160 nL) was incubated with Kinase Buffer (3.84 μL) and the 2X Kinase/Antibody Mixture (8.0 μL). Then, the 4X Tracer was added (4.0 μL) and the plate (Greiner Cat. #784207, bar coded, low volume, white 384-well plate) was shaken for 30 s and incubated for 60 min at room temperature. The plate was read on fluorescence plate reader and analyzed. A known inhibitor (staurosporine) was used as a control.

3.2.2. CDC7 inhibition (ATP-competitive assays)

The ADP-Glo™ Kinase Assay + CDC7/DBF4 Kinase Enzyme System (no. catalog V5089) from Promega was used to determine the activity of selected compounds against CDC7. ATP and other reagents were purchased from Sigma-Aldrich (St. Louis, MO). The assays were performed in a buffer solution using 96-well plates. The compound to be tested (5 μL, 40 μM dissolved in 4% DMSO) was added to each well followed by the enzyme (5 μL, 25 ng/well), ATP (5 μL, final concentration in the well 10 μM) and PDKtide (5 μL, 4 μg/well). Then it was allowed to incubate for 60 min at room temperature and ADP-Glo™ reagent (20 μL) was added allowing to incubate again for 40 min at room temperature. Behind the incubation, the kinase detection agent (40 μL) was added and allowed to incubate for 30 min at room temperature. Finally, the luminescence was recorded using a FLUOstar Optima (BMG Labtechnologies GmbH, Offenburg, Germany) multimode reader. The inhibition activities were calculated based on the maximum activity, measured in the absence of inhibitor. To evaluate the mechanism of CDC7 inhibition of the compounds, ATP-dependent kinetic experiments were performed. CDC7 activity was measured at four different concentrations of ATP (1–100 μM) in the absence or presence of the inhibitors, at two concentrations. The results are presented as double reciprocal Lineweaver–Burk plots (1/*V* vs 1/*S*).

3.2.3. Kinase profiling

The kinase profiling studies were carried out by Life Technologies (Thermo Fisher Scientific) using the appropriate protocol in any case: LRRK2, DAPK1, PIK3C2A (Adapta Assay) [53]; MAPK (LanthaScreen Eu Kinase Binding Assay) [52]; other kinases (Z'-LYTE Assay) [54].

3.2.4. Parallel Artificial Membrane Permeability Assay (PAMPA) Blood-Brain Barrier (BBB)

Prediction of the blood brain barrier penetration was evaluated using a parallel artificial membrane permeability assay (PAMPA) [55]. Ten commercial drugs were used as controls in order to validate the analysis set; Caffeine, Enoxacin, Hydrocortisone, Desipramine, Ofloxacin, Piroxicam, Testosterone, Promazine, Verapamil and Atenolol. Controls and CDC7 inhibitors were dissolved in 1.5 mL of experimental buffer (phosphate buffer saline solution at pH 7.4 (PBS); EtOH (70:30 respectively)). The donor 96-well plate was filled with 180 μL of each filtered compound solution after being coated with 4 μL of porcine brain lipid in dodecane

(20 mg mL⁻¹). The acceptor 96-well plate was filled with 180 µL of experimental buffer. Then the donor plate was carefully placed on the acceptor plate to form a “sandwich” for 2 h and 30 min at 25 °C. During this time, compounds diffused from the donor plate through the brain lipid membrane into the acceptor plate. After incubation, the donor plate was removed. The concentration of compounds and commercial drugs in the acceptor and the donor wells was determined by UV. Every sample was analyzed at three to five wavelengths, in 3 wells and in two independent runs. Results are given as the mean ± standard deviation (SD) of the two runs.

Commercial drugs, phosphate buffer saline solution at pH 7.4 (PBS), Ethanol and dodecane were purchased from Sigma, Acros organics, Merck, Aldrich and Fluka. The porcine polar brain lipid (PBL) (catalog no. 141101) was from Avanti Polar Lipids. The donor plate was a 96-well filtrate plate (Multiscreen® IP Sterile Plate PDVF membrane, pore size is 0.45 µm, catalog no. MAIPS4510) and the acceptor plate was an indented 96-well plate (Multiscreen®, catalog no. MAMCS9610) both from Millipore. To filter the samples Filter PDVF membrane units (diameter 30 mm, pore size 0.45 µm) from Synta were used. A 96-well plate UV reader (Thermo-scientific, Multiskan spectrum) was used for the UV measurements.

3.2.5. Neuronal cell culture

The human neuroblastoma SH-SY5Y cell line was cultured in Dulbecco's Modified Eagle Medium (DMEM) containing L-glutamine (2 mM), 1% non-essential amino acids and supplemented with 10% fetal bovine serum (FBS) and 1% of penicillin/streptomycin in a humidified 5% CO₂ incubator at 37 °C. All components for cell culture were obtained from Invitrogen (Carlsbad, CA, USA).

Cell viability was analyzed in the presence or absence of CDC7 inhibitors in a 96-well plate (60.000 cells/well). Cells were treated at different concentrations of the compounds (5 µM and 10 µM). 24 h after treatment cell survival was measured by the MTT assay (Sigma Aldrich) as previously described [56].

Neuroprotective assay was carried out in a 96-well plate (60.000 cells/well). On attaining semi-confluence cells were exposed to 20 µM of ethacrynic acid (EA) (Sigma Aldrich) for 24 h. Some cultures were pre-treated for 1 h with CDC7 inhibitors (10 µM) or the commercial GSK-3β inhibitor (Tideglusib, 5 µM). Cell viability was determined by the MTT assay. Cell survival was normalized to untreated control cells and represented as a percentage.

3.2.6. Immunoblotting analysis

SH-SY5Y cells (2 × 10⁶ cells/well) were incubated in 6-well plates, harvested, washed with cold PBS and resuspended in cold lysis buffer (50 mM Tris pH 7.4, 1% Nonidet-40 and 150 mM NaCl). Spinal cord samples were lysed in RIPA buffer supplemented with a protease and phosphatase inhibitor cocktail. Protein content of samples was measured with Pierce BCA Protein Assay Kit (Thermo Scientific). 20–50 µg of protein were fractioned on a 10% SDS polyacrylamide gel (Bio-Rad) and transferred to poly-vinylidene fluoride (PVDF) membranes (Millipore, Billerica, MA, USA) at 4 °C. The membranes were then blocked with 5% of Bovine Serum Albumin (BSA, Sigma Aldrich) in spinal cord and SH-SY5Y cells samples, for 1 h. Membranes were incubated overnight at 4 °C with the following primary antibodies: phospho-(S403-404)-TDP-43 monoclonal (1:500, Proteintech); anti-TDP-43 (1:800 Proteintech) and α-tubulin (1:1000, Santa Cruz Biotechnology). Primary antibodies signal was amplified with species-specific antisera antibodies conjugated with horseradish peroxidase (Bio-Rad) and detected with a chemiluminescent substrate detection system ECL (Thermo Scientific). Relative band intensities were quantified using a ChemiDoc station with Quantity One 1D analysis software (Bio-Rad).

3.2.7. Immunofluorescence analysis

Cells were permeabilized with 0.25% Triton X-100 10% (Sigma Aldrich) for 10 min at RT and blocked with 0.1% of casein and 2% of BSA (Sigma Aldrich) for 30 min at RT. Then cells were incubated with TDP-43 antibody (1:800, Proteintech) in 6% BSA for 1 h at 37 °C. After removing the primary antibody, cells were incubated with Alexa Fluor 488 conjugate secondary antibody (1:600, Jackson Immuno Research) for 1 h. Cell nuclei were stained using HCS NuclearMask Deeo Red (1:250, Thermo Fisher) for 30 min and then washed twice with 1% BSA and 0.1% casein and rinsed with PBS three times. Finally, preparations were mounted onto Fluoromount Mounting Medium (Sigma Aldrich). Images were obtained using a Confocal Laser Scanning Microscopy (CLMS) Leica TCS SP8 with 63x oil immersion objective. TDP43 levels were quantified using ImageJ software. Data is expressed at the ratio of the fluorescence intensity of cytosolic TDP43 vs nuclear TDP-43.

3.2.8. CDC7 inhibitor assays in *C. elegans*

C. elegans strain CK423 *bus-8(e2698); bkl5423[Psnb-1:hTDP-43 + myo-2::dsRED]* was used for screening [19]. The cuticle-defective *bus-8(e2692)* mutation is included to enhance small molecule entry into the animals [57]. To conduct the screen, 6 mL of nematode growth medium (NGM) were added into 60 mm culture dishes. Each well was seeded with 200 µL of 10x concentrated OP-50 *E. coli*. After the bacterial lawn dried, bacteria were killed by UV irradiation to minimize metabolism of test compounds by live bacteria. Serial dilutions in DMSO of each drug in 40 µL total volumes were added to each plate, to the indicated final concentrations. Approximately 100 *C. elegans* eggs were plated and grown for 6 days at 20 °C, then harvested. *C. elegans* protein immunoblotting was performed as previously described [58]. Samples were loaded and resolved on precast 4–15% gradient SDS-PAGE gels and transferred to PVDF membrane as recommended by the manufacturer (Bio-Rad). On immunoblots, TDP-43 phosphorylated at S409/S410 was detected by a monoclonal antibody anti-phospho TDP-43 (pS409/410) (Cosmobio TIP-PTD-M01). *C. elegans* β-tubulin levels were measured using monoclonal antibody E7 (Developmental Studies Hybridoma Bank) as a loading control. Dilutions for all primary antibodies were: 1:5000. HRP labeled goat anti-mouse IgG was the secondary antibody (Jackson ImmunoResearch) and used at a dilution of 1:5000.

3.2.9. Animal procedures, treatment and sampling

All experimental procedures were conducted according to protocols approved by the ethical committees of the Complutense University and the regulatory institution (ref. PROEX 059/16) in accordance with the European Commission regulations (2010/63/EU). Wild-type and Prp-hTDP-43(A315T) transgenic littermate sibling mice were bred in house from initial breeders purchased from Jackson Laboratories (Bar Harbor, ME, USA). Mice were maintained on a 12 h light/dark cycle in a temperature-controlled atmosphere (22 ± 1 °C) with food and water ad libitum. Offspring were genotyped as previously described [44], and male mice randomly divided into four groups (*n* = 8). Compound **22** was dissolved in 2.9% DMSO and Tween 80-saline buffer (1:16) and administered intraperitoneally, starting at the age of 65 days old, at a dose of 5 mg/kg daily until sacrifice at the age of 95 days old. Vehicle injections were administered to control animals. During all the treatment, we also recorded the physical appearance and the animal weight gain. After 30 days of chronic treatment wild-type and Prp-hTDP-43 (A315T) transgenic mice were sacrificed 24 h after the last injection. Spinal cords were rapidly collected and flash-frozen in 2-methylbutane cooled in dry ice and stored at -80 °C.

3.2.10. Behavioral evaluation

Mice were subjected to different behavioral test for determining their neurological status. All behavioral test were conducted prior to drug injection to avoid acute effects of the compound administered. We evaluated motor function in Prp-hTDP-43 (A315T) transgenic and wild-type mice using the rotarod test, a LE8200 device (Panlab, Barcelona, Spain). After a period of acclimation and training (first session: 0 r.p.m. for 30 s; second and third sessions: 4 r.p.m. for 60 s, with periods of 10 min between sessions) conducted 30 min before, animals were tested with an acceleration from 4 to 40 r.p.m. over a period of 300 s. Mice were tested for three consecutive trials with a rest period of approximately 15 min between trials and the mean of the three trials was calculated.

To analyze animals for the hindlimb clasp reflex, mice were lifted on the base of their tail and animals were scored according to the following scale: (i) score = 0 if the hindlimbs are consistently splayed outward, away from the abdomen; (ii) score = 1 if one hindlimb is retracted toward the abdomen; (iii) score = 2 if both hindlimbs are partially retracted toward the abdomen; and (iv) score = 3 if both hindlimbs are entirely retracted and touching the abdomen. The data for each experimental group corresponds to the average of three tests.

3.2.11. Statistical analysis

Graph Pad Prism 6 (La Jolla, CA, USA) was used for statistical analysis. All quantitative data are presented as the mean \pm SEM from independent experiments. One-way ANOVA followed by the Newman-Keuls or Dunnett's multiple comparisons tests were used in order to estimate the statistical significance. A *P* value lower than 0.05 was set as the limit for statistical significance.

Declaration of competing interest

The authors declare that they have no known competing financial interests or personal relationships that could have appeared to influence the work reported in this paper.

Acknowledgements

This work was supported by Comunidad de Madrid (grant B2017/BMD-3813), MINECO (grant SAF2016-76693-R and PID2019-105600RB-I00 to A.M., RTI2018-0988885-B-I00 to E.d.L. and CTQ2015-66313-R to A.M.R.), ISCIII CIBERNED (CB18/05/00040 to A.M., C.G. and A.M.R. and CB06/05/0089 to E.d.L.), MEC (FPU14-00204 to E.R.), the National Institutes of Health (R01NS064131 to B.C.K.) and the Department of Veterans Affairs (Merit Review Grants I01BX003755 to B.C.K. and I01BX004044 to N.F.L.), CONICYT-PCI (grant REDES190074 to D.R. and A.M.) and FONDECYT (grant no. 11180604 to D.R.). We thank Heather Currey, Josh Hincks and Carlota Tosat-Bribian for essential technical assistance.

Appendix A. Supplementary data

Superposition x-ray complex and docking model for AD and PH; correlation plot between predicted ΔG_{bind} and experimental CDC7 IC₅₀ values; experimental permeability data in the PAMPA-BBB assay; linear correlation between experimental and reported permeability of commercial drugs using the PAMPA-BBB assay; viability studies for CDC7 inhibitors; body weight evolution of TDP-43 and wild-type mice during the 30 days of treatment with CDC7 inhibitor or vehicle; synthesis and structural characterization of compounds **1–7**, **7b**, **9–10**, **12**, **14**, **20**, **30–32**, **34** and **36**.

Supplementary data to this article can be found online at <https://doi.org/10.1016/j.ejmech.2020.112968>.

References

- [1] S. Zarei, K. Carr, L. Reiley, K. Diaz, O. Guerra, P.F. Altamirano, W. Pagani, D. Lodin, G. Orozco, A. China, A comprehensive review of amyotrophic lateral sclerosis, *Surg. Neurol. Int.* 6 (2015) 171.
- [2] A. Al-Chalabi, O. Hardiman, The epidemiology of ALS: a conspiracy of genes, environment and time, *Nat. Rev. Neurol.* 9 (2013) 617–628.
- [3] A. McGown, M.J. Stopford, High-throughput drug screens for amyotrophic lateral sclerosis drug discovery, *Expert Opin. Drug Discov.* 13 (2018) 1015–1025.
- [4] S.M. Chou, H.S. Wang, K. Komai, Colocalization of NOS and SOD1 in neurofilament accumulation within motor neurons of amyotrophic lateral sclerosis: an immunohistochemical study, *J. Chem. Neuroanat.* 10 (1996) 249–258.
- [5] J.P. Julien, J. Kriz, Transgenic mouse models of amyotrophic lateral sclerosis, *Biochim. Biophys. Acta* 1762 (2006) 1013–1024.
- [6] M.A. White, J. Sreedharan, Amyotrophic lateral sclerosis: recent genetic highlights, *Curr. Opin. Neurol.* 29 (2016) 557–564.
- [7] E.N. Guerrero, H. Wang, J. Mitra, P.M. Hegde, S.E. Stowell, N.F. Liachko, B.C. Kraemer, R.M. Garruto, K.S. Rao, M.L. Hegde, TDP-43/FUS in motor neuron disease: complexity and challenges, *Prog. Neurobiol.* 145–146 (2016) 78–97.
- [8] R.H. Tan, J.J. Kril, M. Fatima, A. McGeachie, H. McCann, C. Shepherd, S.L. Forrest, A. Affleck, J.B. Kwok, J.R. Hodges, M.C. Kiernan, G.M. Halliday, TDP-43 proteinopathies: pathological identification of brain regions differentiating clinical phenotypes, *Brain* 138 (2015) 3110–3122.
- [9] E. Buratti, TDP-43 post-translational modifications in health and disease, *Expert Opin. Ther. Targets* 22 (2018) 279–293.
- [10] J. Gao, L. Wang, M.L. Huntley, G. Perry, X. Wang, Pathomechanisms of TDP-43 in neurodegeneration, *J. Neurochem.* 146 (2018) 7–20.
- [11] V. Palomo, C. Tosat-Bitrian, V. Nozal, S. Nagaraj, A. Martin-Requero, A. Martinez, TDP-43: a key therapeutic target beyond amyotrophic lateral sclerosis, *ACS Chem. Neurosci.* 10 (2019) 1183–1196.
- [12] S. Gross, R. Rahal, N. Stransky, C. Lengauer, K.P. Hoeflich, Targeting cancer with kinase inhibitors, *J. Clin. Invest.* 125 (2015) 1780–1789.
- [13] S. Klaeger, S. Heinzlmeir, M. Wilhelm, H. Polzer, B. Vick, P.A. Koenig, M. Reinecke, B. Ruprecht, S. Petzoldt, C. Meng, J. Zecha, K. Reiter, H. Qiao, D. Helm, H. Koch, M. Schoof, G. Canevari, E. Casale, S.R. Depaolini, A. Feuchtinger, Z. Wu, T. Schmidt, L. Rueckert, W. Becker, J. Huenges, A.K. Garz, B.O. Gohlke, D.P. Zolg, G. Kayser, T. Voeder, R. Preissner, H. Hahne, N. Tonisson, K. Kramer, K. Gotze, F. Bassermann, J. Schlegl, H.C. Ehrlich, S. Aiche, A. Walch, P.A. Greif, S. Schneider, E.R. Felder, J. Ruland, G. Medard, I. Jeremias, K. Spiekermann, B. Kuster, The target landscape of clinical kinase drugs, *Science* 358 (2017), eaan4368.
- [14] F. Kametani, T. Nonaka, T. Suzuki, T. Arai, N. Dohmae, H. Akiyama, M. Hasegawa, Identification of casein kinase-1 phosphorylation sites on TDP-43, *Biochem. Biophys. Res. Commun.* 382 (2009) 405–409.
- [15] I.G. Salado, M. Redondo, M.L. Bello, C. Perez, N.F. Liachko, B.C. Kraemer, L. Miguel, M. Lecourtois, C. Gil, A. Martinez, D.I. Perez, Protein kinase CK-1 inhibitors as new potential drugs for amyotrophic lateral sclerosis, *J. Med. Chem.* 57 (2014) 2755–2772.
- [16] L. Martinez-Gonzalez, C. Rodriguez-Cueto, D. Cabezudo, F. Bartolome, P. Andres-Benito, I. Ferrer, C. Gil, A. Martin-Requero, J. Fernandez-Ruiz, A. Martinez, E. de Lago, Motor neuron preservation and decrease of in vivo TDP-43 phosphorylation by protein CK-1delta kinase inhibitor treatment, *Sci. Rep.* 10 (2020) 4449.
- [17] C. Alquezar, I.G. Salado, A. de la Encarnacion, D.I. Perez, F. Moreno, C. Gil, A.L. de Munain, A. Martinez, A. Martin-Requero, Targeting TDP-43 phosphorylation by Casein Kinase-1delta inhibitors: a novel strategy for the treatment of frontotemporal dementia, *Mol. Neurodegener.* 11 (2016) 36.
- [18] D. Posa, L. Martinez-Gonzalez, F. Bartolome, S. Nagaraj, G. Porras, A. Martinez, A. Martin-Requero, Recapitulation of pathological TDP-43 features in immortalized lymphocytes from sporadic ALS patients, *Mol. Neurobiol.* 56 (2019) 2424–2432.
- [19] N.F. Liachko, P.J. McMillan, C.R. Guthrie, T.D. Bird, J.B. Leverenz, B.C. Kraemer, CDC7 inhibition blocks pathological TDP-43 phosphorylation and neurodegeneration, *Ann. Neurol.* 74 (2013) 39–52.
- [20] L.M. Taylor, P.J. McMillan, N.F. Liachko, T.J. Strovas, B. Ghetti, T.D. Bird, C.D. Keene, B.C. Kraemer, Pathological phosphorylation of tau and TDP-43 by TTBK1 and TTBK2 drives neurodegeneration, *Mol. Neurodegener.* 13 (2018) 7.
- [21] R. Swords, D. Mahalingam, M. O'Dwyer, C. Santocanale, K. Kelly, J. Carew, F. Giles, Cdc7 kinase - a new target for drug development, *Eur. J. Canc.* 46 (2010) 33–40.
- [22] N.K. Sasi, K. Tiwari, F.F. Soon, D. Bonte, T. Wang, K. Melcher, H.E. Xu, M. Weinreich, The potent Cdc7-Dbf4 (DDK) kinase inhibitor XL413 has limited activity in many cancer cell lines and discovery of potential new DDK inhibitor scaffolds, *PLoS One* 9 (2014), e113300.
- [23] M. Menichincheri, C. Albanese, C. Allii, D. Ballinari, A. Bargiotti, M. Caldarelli, A. Ciavolella, A. Cirila, M. Colombo, F. Colotta, V. Croci, R. D'Alessio, M. D'Anello, A. Ermoli, F. Fiorentini, B. Forte, A. Galvani, P. Giordano, A. Isacchi, K. Martina, A. Molinari, J.K. Moll, A. Montagnoli, P. Orsini, F. Orzi, E. Pesenti, A. Pillan, F. Roletto, A. Sclaro, M. Tato, M. Tibolla, B. Valsasina, M. Varasi, P. Vianello, D. Volpi, C. Santocanale, E. Vanotti, Cdc7 kinase inhibitors: 5-heteroaryl-3-carboxamido-2-aryl pyrroles as potential antitumor agents. 1. Lead finding, *J. Med. Chem.* 53 (2010) 7296–7315.
- [24] T. Shimizu, T. Doi, S. Kondo, H. Takahashi, N. Yamamoto, E. Sheldon-Waniga,

- X. Zhou, B. Bahamon, H. Li, Y. Kuboki, First-in-human phase 1 study of TAK-931, an oral cell division cycle 7 (CDC7) inhibitor, in patients (pts) with advanced solid tumors, *J. Clin. Oncol.* 36 (2018) 2506.
- [25] A. Natoni, M.R. Coyne, A. Jacobsen, M.D. Rainey, G. O'Brien, S. Healy, A. Montagnoli, J. Moll, M. O'Dwyer, C. Santocanale, Characterization of a dual CDC7/Cdk9 inhibitor in multiple myeloma cellular models, *Cancers* 5 (2013) 901–918.
- [26] C.S. Lebakken, S.M. Riddle, U. Singh, W.J. Frazee, H.C. Eliason, Y. Gao, L.J. Reichling, B.D. Marks, K.W. Vogel, Development and applications of a broad-coverage, TR-FRET-based kinase binding assay platform, *J. Biomol. Screen* 14 (2009) 924–935.
- [27] V. Sebastian-Perez, C. Roca, M. Awale, J.L. Reymond, A. Martinez, C. Gil, N.E. Campillo, Medicinal and Biological Chemistry (MBC) library: an efficient source of new hits, *J. Chem. Inf. Model.* 57 (2017) 2143–2151.
- [28] H. Masai, K. Arai, Dbf4 motifs: conserved motifs in activation subunits for Cdc7 kinases essential for S-phase, *Biochem. Biophys. Res. Commun.* 275 (2000) 228–232.
- [29] M.W. Karaman, S. Herrgard, D.K. Treiber, P. Gallant, C.E. Atteridge, B.T. Campbell, K.W. Chan, P. Ciceri, M.I. Davis, P.T. Edeen, R. Faraoni, M. Floyd, J.P. Hunt, D.J. Lockhart, Z.V. Milanov, M.J. Morrison, G. Pallares, H.K. Patel, S. Pritchard, L.M. Wodicka, P.P. Zarrinkar, A quantitative analysis of kinase inhibitor selectivity, *Nat. Biotechnol.* 26 (2008) 127–132.
- [30] M. Sawa, H. Masai, Drug design with Cdc7 kinase: a potential novel cancer therapy target, *Drug Des. Dev. Ther.* 2 (2009) 255–264.
- [31] S. Hughes, F. Elustondo, A. Di Fonzo, F.G. Leroux, A.C. Wong, A.P. Snijders, S.J. Matthews, P. Cherepanov, Crystal structure of human CDC7 kinase in complex with its activator DBF4, *Nat. Struct. Mol. Biol.* 19 (2012) 1101–1107.
- [32] Y.A. Rodriguez, M. Gutierrez, D. Ramirez, J. Alzate-Morales, C.C. Bernal, F.M. Guiza, A.R. Romero Bohorquez, Novel N-allyl/propargyl tetrahydroquinolines: synthesis via three-component cationic imino Diels-Alder reaction, binding prediction, and evaluation as cholinesterase inhibitors, *Chem. Biol. Drug Des.* 88 (2016) 498–510.
- [33] C. Mulakala, V.N. Viswanadhan, Could MM-GBSA be accurate enough for calculation of absolute protein/ligand binding free energies? *J. Mol. Graph. Model.* 46 (2013) 41–51.
- [34] A. Montagnoli, B. Valsasina, V. Croci, M. Menichincheri, S. Rainoldi, V. Marchesi, M. Tibolla, P. Tenca, D. Brotherton, C. Albanese, V. Patton, R. Alzani, A. Ciavolella, F. Sola, A. Molinari, D. Volpi, N. Avanzi, F. Fiorentini, M. Cattoni, S. Healy, D. Ballinari, E. Pesenti, A. Isacchi, J. Moll, A. Bensimon, E. Vanotti, C. Santocanale, A Cdc7 kinase inhibitor restricts initiation of DNA replication and has antitumor activity, *Nat. Chem. Biol.* 4 (2008) 357–365.
- [35] W. Li, X.L. Zhao, S.Q. Shang, H.Q. Shen, X. Chen, Dual inhibition of Cdc7 and Cdk9 by PHA-767491 suppresses hepatocarcinoma synergistically with 5-fluorouracil, *Curr. Cancer Drug Targets* 15 (2015) 196–204.
- [36] P. Crivori, G. Cruciani, P.A. Carrupt, B. Testa, Predicting blood-brain barrier permeation from three-dimensional molecular structure, *J. Med. Chem.* 43 (2000) 2204–2216.
- [37] Y. Iguchi, M. Katsuno, S. Takagi, S. Ishigaki, J. Niwa, M. Hasegawa, F. Tanaka, G. Sobue, Oxidative stress induced by glutathione depletion reproduces pathological modifications of TDP-43 linked to TDP-43 proteinopathies, *Neurobiol. Dis.* 45 (2012) 862–870.
- [38] G. Vaca, L. Martinez-Gonzalez, E. Rojas-Prats, G. Porras, E.P. Cuevas, C. Gil, A. Martinez, A. Martin-Requero, Therapeutic potential of novel Cell Division Cycle Kinase 7 inhibitors on TDP-43-related pathogenesis such as Frontotemporal Lobar Degeneration (FTLD) and amyotrophic lateral sclerosis (ALS), *J. Neurochem.* (2020), <https://doi.org/10.1111/jnc.15118>.
- [39] N.F. Liachko, C.R. Guthrie, B.C. Kraemer, Phosphorylation promotes neurotoxicity in a *Caenorhabditis elegans* model of TDP-43 proteinopathy, *J. Neurosci.* 30 (2010) 16208–16219.
- [40] J.G. White, E. Southgate, J.N. Thomson, S. Brenner, The structure of the nervous system of the nematode *Caenorhabditis elegans*, *Philos. Trans. R. Soc. Lond. B Biol. Sci.* 314 (1986) 1–340.
- [41] A.D. Chisholm, S. Xu, The *Caenorhabditis elegans* epidermis as a model skin. II: differentiation and physiological roles, *Wiley Interdiscip. Rev. Dev. Biol.* 1 (2012) 879–902.
- [42] J.B. Rand, C.D. Johnson, Genetic pharmacology: interactions between drugs and gene products in *Caenorhabditis elegans*, *Methods Cell Biol.* 48 (1995) 187–204.
- [43] A.R. Schwendeman, S. Shaham, A High-throughput small molecule screen for *C. elegans* linker cell death inhibitors, *PLoS One* 11 (2016), e0164595.
- [44] I. Węgorzewska, S. Bell, N.J. Cairns, T.M. Miller, R.H. Baloh, TDP-43 mutant transgenic mice develop features of ALS and frontotemporal lobar degeneration, *Proc. Natl. Acad. Sci. U. S. A.* 106 (2009) 18809–18814.
- [45] P.T. Nelson, D.W. Dickson, J.Q. Trojanowski, C.R. Jack, P.A. Boyle, K. Arfanakis, R. Rademakers, I. Alafuzoff, J. Attems, C. Brayne, I.T.S. Coyle-Gilchrist, H.C. Chui, D.W. Fardo, M.E. Flanagan, G. Halliday, S.R.K. Hokkanen, S. Hunter, G.A. Jicha, Y. Katsumata, C.H. Kawas, C.D. Keene, G.G. Kovacs, W.A. Kukull, A.I. Levey, N. Makinejad, T.J. Montine, S. Murayama, M.E. Murray, S. Nag, R.A. Rissman, W.W. Seeley, R.A. Sperling, C.L. White III, L. Yu, J.A. Schneider, Limbic-predominant age-related TDP-43 encephalopathy (LATE): consensus working group report, *Brain* 142 (2019) 1503–1527.
- [46] G.H. Hitchings, G.B. Elion, G. Irving, 6-Benzylmercaptapurines, U. S. Patent 3 937 (1966) 232.
- [47] R.A. Friesner, J.L. Banks, R.B. Murphy, T.A. Halgren, J.J. Klicic, D.T. Mainz, M.P. Repasky, E.H. Knoll, M. Shelley, J.K. Perry, D.E. Shaw, P. Francis, P.S. Shenkin, Glide: a new approach for rapid, accurate docking and scoring. 1. Method and assessment of docking accuracy, *J. Med. Chem.* 47 (2004) 1739–1749.
- [48] T.A. Halgren, R.B. Murphy, R.A. Friesner, H.S. Beard, L.L. Frye, W.T. Pollard, J.L. Banks, Glide: a new approach for rapid, accurate docking and scoring. 2. Enrichment factors in database screening, *J. Med. Chem.* 47 (2004) 1750–1759.
- [49] Schrödinger Suite 2016-1 Including Protein Preparation Wizard, Epik, Impact, and Prime, Schrödinger LLC, New York, NY, 2016.
- [50] G.M. Sastry, M. Adzhigirey, T. Day, R. Annabhimoju, W. Sherman, Protein and ligand preparation: parameters, protocols, and influence on virtual screening enrichments, *J. Comput. Aided Mol. Des.* 27 (2013) 221–234.
- [51] R.A. Friesner, R.B. Murphy, M.P. Repasky, L.L. Frye, J.R. Greenwood, T.A. Halgren, P.C. Sanschagrin, D.T. Mainz, Extra precision glide: docking and scoring incorporating a model of hydrophobic enclosure for protein-ligand complexes, *J. Med. Chem.* 49 (2006) 6177–6196.
- [52] <https://www.thermofisher.com/es/es/home/industrial/pharma-biopharma/drug-discovery-development/target-and-lead-identification-and-validation/kinasebiology/kinase-activity-assays/lanthascreentm-eu-kinase-binding-assay.html>. (Accessed 26 May 2020).
- [53] <https://www.thermofisher.com/es/es/home/industrial/pharma-biopharma/drug-discovery-development/target-and-lead-identification-and-validation/kinasebiology/kinase-activity-assays/adapta-universal-kinase-assay.html>. (Accessed 26 May 2020).
- [54] <https://www.thermofisher.com/es/es/home/industrial/pharma-biopharma/drug-discovery-development/target-and-lead-identification-and-validation/kinasebiology/kinase-activity-assays/z-lyte.html>. (Accessed 26 May 2020).
- [55] L. Di, E.H. Kerns, K. Fan, O.J. McConnell, G.T. Carter, High throughput artificial membrane permeability assay for blood-brain barrier, *Eur. J. Med. Chem.* 38 (2003) 223–232.
- [56] F. Denizot, R. Lang, Rapid colorimetric assay for cell growth and survival. Modifications to the tetrazolium dye procedure giving improved sensitivity and reliability, *J. Immunol. Methods* 89 (1986) 271–277.
- [57] F.A. Partridge, A.W. Tearle, M.J. Gravato-Nobre, W.R. Schafer, J. Hodgkin, The *C. elegans* glycosyltransferase BUS-8 has two distinct and essential roles in epidermal morphogenesis, *Dev. Biol.* 317 (2008) 549–559.
- [58] N.F. Liachko, A.D. Saxton, P.J. McMillan, T.J. Strovos, H.N. Currey, L.M. Taylor, J.M. Wheeler, A.L. Oblak, B. Ghetti, T.J. Montine, C.D. Keene, M.A. Raskind, T.D. Bird, B.C. Kraemer, The phosphatase calcineurin regulates pathological TDP-43 phosphorylation, *Acta Neuropathol.* 132 (2016) 545–561.